

# The properties of field elliptical galaxies at intermediate redshift. III: the Fundamental Plane and the evolution of stellar populations from $z = 0.4$ to $z = 0$ .

T. Treu,<sup>1,2,4</sup> M. Stiavelli,<sup>2</sup> G. Bertin,<sup>1</sup> S. Casertano<sup>2</sup> and P. M. Ller<sup>3</sup>

<sup>1</sup> Scuola Normale Superiore, P.zza dei Cavalieri 7, I-56126, Pisa, Italy

<sup>2</sup> Space Telescope Science Institute, 3700 San Martin Dr., Baltimore, MD 21218, USA

<sup>3</sup> ESO, Karl-Schwarzschild Str. 2, D 85748, Garching bei München, Germany

<sup>4</sup> present address: California Institute of Technology, Astronomy 105-24, Pasadena, CA 91125, USA; e-mail tt@astro.caltech.edu

10 April 2024

## ABSTRACT

We report on the study of a sample of 25 field early-type galaxies, in the redshift range  $z = 0.1 - 0.5$ , selected on the basis of colours and morphology from the Medium Deep Survey (MDS) of the Hubble Space Telescope (HST). Surface photometry in two colors (F606W and F814W) and redshifts have been derived for all the galaxies in the sample, while velocity dispersions have been measured for 19 of the sample galaxies, as described in a companion paper.

Our study of the evolution of the Fundamental Plane (FP) with redshift yields the following results. Field early-type galaxies define a tight FP out to  $z = 0.4$ , with scatter unchanged with respect to local samples, within the observational errors. The intermediate redshift FP is offset with respect to the local FP of the Coma Cluster, in the sense that, for given effective radius and velocity dispersion, galaxies are brighter than expected from the local relation. The offset of the FP is found to increase with redshift. The range of parameters covered by our sample is not sufficiently extended to measure the slopes of the FP at intermediate redshift. Similar results are found for the  $SB_e-R_e$  relation, out to  $z = 0.5$ .

The evolution of the FP (and of the  $SB_e-R_e$  relation) is studied quantitatively with a Bayesian-Monte Carlo technique. By applying this technique, we find that the offset of the intercept of the FP ( $\beta$ ) with respect to the local FP increases as  $\beta = z$  with the following 68 per cent limits:  $0.33 < \beta < 0.44$  (for  $\beta = 1$ ;  $\beta = 0$ ) or  $0.44 < \beta < 0.56$  (for  $\beta = 0.3$ ;  $\beta = 0.7$ ). In addition, we interpret the results in terms of the evolution of the stellar populations, under the assumption of passive evolution. In a single-burst scenario, the observed properties are consistent with those of a stellar population formed at  $z > 2$  (for  $\beta = 1$ ;  $\beta = 0$ ,  $H_0 = 50 \text{ km s}^{-1} \text{ Mpc}^{-1}$ ) or  $0.8 < z < 1.6$  (for  $\beta = 0.3$ ;  $\beta = 0.7$ ,  $H_0 = 65 \text{ km s}^{-1} \text{ Mpc}^{-1}$ ). If a small fraction of the stellar mass is formed in a secondary burst, the primary burst may have occurred at higher  $z$ . For example (for  $\beta = 0.3$ ;  $\beta = 0.7$ ,  $H_0 = 65 \text{ km s}^{-1} \text{ Mpc}^{-1}$ ) the primary burst may have occurred at  $z > 3$  if a secondary burst with a tenth of stellar mass occurred at  $0.6 < z < 0.8$ .

Finally, the intercept and scatter of the FP found for field early-type galaxies and for cluster data (taken from the literature) at  $z = 0.3 - 0.4$  are mutually consistent, within the observational errors. If higher redshift (up to  $z = 0.83$ ) cluster data are considered, the ages of the stellar populations of field early-type galaxies inferred from a single-burst scenario are found to be marginally smaller than the ages derived for the cluster galaxies.

**Key words:**

galaxies: elliptical and lenticular, cD | galaxies: evolution | galaxies: photometry | galaxies: kinematics and dynamics | galaxies: fundamental parameters | galaxies: formation

arXiv:astro-ph/0106147v1 8 Jun 2001

## 1 INTRODUCTION

Despite the progress made in understanding the physics of early-type galaxies (E/S0), a single widely accepted model, capable of explaining all their observed properties, is not yet available. A variety of scenarios are still considered to be viable (see e.g. Larson 1975, Toomre 1977, van Albada 1982). Schematically, we can identify the following two main classes of scenarios. In the traditional view, the monolithic collapse scenario, E/S0 form in a rapid collapse shortly after an intense burst of star formation. Since the stellar populations of E/S0 in the local Universe are generally old, and no such intense bursts of star formation are observed at redshift  $z < 1$ , it is generally assumed that most of these monolithic collapse events occurred at high redshifts. In the alternate view, the merging scenario, E/S0 form by interactions of disc galaxies. The merging scenario has been cast into a cold dark matter cosmological framework, the hierarchical clustering scenario (White & Rees 1978; Kauman, White & Guiderdoni 1993). In the hierarchical clustering scenario the formation of massive E/S0 by merging of discs is a relatively recent phenomenon (Kauman 1996).

In the absence of a satisfactory theoretical scenario, new observations play a key role, by providing additional input and the opportunity to test predictions. Since the theoretical models have been conceived and ‘calibrated’ in order to reproduce the properties of local galaxies, the observation of intermediate ( $0.1 < z < 1$ ) and high redshift ( $z > 1$ ) galaxies is particularly important.

Several observational results have been obtained on this subject in recent years. Most of them have been obtained for the cluster environment, where early-type galaxies are more abundant and studied more efficiently (Ellis et al. 1997; Dressler et al. 1997; Stanford, Eisenhardt & Dickinson, 1998; van Dokkum et al. 1998a,b; Brown et al. 2000; Kelson et al. 2000b; van Dokkum et al. 2000). These studies indicate that the stellar populations of early-type galaxies in the core of rich clusters have possibly formed at high redshift, earlier than  $z \approx 2-3$ .

When comparing intermediate redshift E/S0 to local ones, one should take into account the evolution with redshift of clusters and of the population of galaxies in clusters. Although the evolution of clusters of galaxies is still somewhat controversial (Postman et al. 1996), it is likely that the population of galaxies in clusters evolves by encroaching on isolated galaxies and small groups. Thus, part of the progenitors of present-day cluster E/S0 were likely located outside clusters in the past. Therefore, to gain a reliable global picture, it is necessary to study the evolution of E/S0 in all environments, from the core of rich clusters to the field. In addition, E/S0 have been observed to be subject to interactions with their environment ranging from weak distant encounters to major merging events. Thus, since the frequency of interactions depends upon the environment, evolution should depend upon the environment as well, if interactions play a significant role. For this reason, the role of environment should be especially important in the merging scenario. In the hierarchical clustering scenario, numerical simulations predict (Kauman 1996) that field E/S0 should have younger stars than cluster ones and have assembled later. Therefore, the comparison of the evolution of

the properties of cluster and field E/S0 provides a test of a prediction of hierarchical clustering models.

So far, only a few studies of field early-type galaxies, based on HST high resolution images, have been published (Im et al. 1996; Treu & Stiavelli 1999; Schade et al. 1999; Menanteau et al. 1999; Brinchmann & Ellis 2000), often with very limited statistics (e.g. the analysis of early-type galaxies in the Hubble Deep Fields, Franceschini et al. 1998; Benítez et al. 1999; Kodama, Bower & Bell, 1999; see also Treu et al. 1999). One important result is that field early-type galaxies at intermediate redshifts span a wider range of colours than cluster ones (more extended to the blue; Schade et al. 1999). This is likely to result from a more complex evolution of the stellar populations, with episodes of star formation occurring at lower redshifts than in clusters (see e.g. Trager et al. 2000a,b). A detailed study of the star formation history of field E/S0 is needed to clarify this issue.

A correct picture of the evolution of stellar populations is also needed in order to understand how the number density of E/S0 evolves with redshift. In fact, several studies (Treu & Stiavelli 1999; Menanteau et al. 1999) find that the number of red morphologically selected E/S0 at high  $z$  is smaller than what is predicted by models based on passive luminosity evolution and constant comoving density models. However, Schade et al. (1999) find that the number density of early-type galaxies, selected purely on morphology without color criteria, is consistent with being constant from  $z \approx 1$  to  $z \approx 0.2$  (see also Im et al. 1996). Similarly, Menanteau et al. (1999) find that, if all E/S0 are considered (including the blue ones), the data are consistent with no evolution of the number density.

The evolutionary history of E/S0 derived from the data depends critically on the detailed star formation history involved (for other sources of uncertainties see, e.g., Chiba & Yoshii 1999; Schade et al. 1999; Barger et al. 1999; Daddi et al. 2000). In fact, even otherwise negligible amounts of young stars are sufficient to make high  $z$  E/S0 appear blue and thus to produce the observed ‘decline’ of red high- $z$  E/S0 (Treu & Stiavelli 1999; see also Jimenez et al. 1999 and Abraham et al. 1999).

More detailed spectroscopic information is needed to study the evolution with redshift of the structural properties of E/S0 and of their stellar populations. For this reason we have initiated (Treu et al. 1999; hereafter T99) an observational project aimed at obtaining high signal-to-noise medium resolution spectra for a sample of field early-type galaxies at intermediate redshift selected on the basis of HST-WFPC2 images. The photometric and kinematic measurements for the entire sample ( $0.1 < z < 0.6$ ) are described in a companion paper (Treu et al. 2001; hereafter P II). In the present paper, the third of the series, we study the evolution with redshift of the Fundamental Plane (Dressler et al. 1987; Djorgovski and Davis 1987), a very tight empirical correlation between the main observables of E/S0 (Section 2). Its existence and tightness have profound implications in terms of galactic formation and evolution, and it is therefore particularly interesting to investigate how far in the past it exists and what is the time evolution of its coefficients and scatter. In addition, the Fundamental Plane is used as a diagnostic of stellar populations, to study the star formation history of field E/S0. A similar study is performed on the evolution of the  $SB_e-R_e$  relation (Kormendy

1977; Section 4.2), a photometric projection of the Fundamental Plane. Future papers will report on the measurement of ages and metallicity, using the absorption line indices in the Lick/IDS system (Trager et al. 1998).

The paper is organized as follows. The Fundamental Plane as a diagnostic tool of the stellar populations is described in Section 2. In Section 3 we give a brief summary of the data described in P II. In Section 4 we illustrate the observational results, i.e. we discuss the existence and location of the intermediate redshift field Fundamental Plane. In Section 5 we analyse selection effects that must be taken into account while interpreting the results in terms of stellar population evolution (Section 6). In Section 7 we compare the Fundamental Plane of field early-type galaxies to the Fundamental Plane of clusters at similar redshift, with data and results taken from the literature. Conclusions are drawn in Section 8.

The results presented here are given for two sets of values of the cosmological parameters (the matter density and the cosmological constant, expressed in dimensionless form, and the Hubble constant  $H_0 = 50 h_{50} \text{ km s}^{-1} \text{ Mpc}^{-1}$ ): a long lived Universe ( $\Omega = 0.3$ ,  $\Omega_\Lambda = 0.7$ ,  $h_{50} = 1.30$ ; age of the Universe  $14.6 \text{ Gyr}$ ) and the ‘classical choice’ of parameters ( $\Omega = 1$ ,  $\Omega_\Lambda = 0$ ,  $h_{50} = 1$ ; age of the Universe  $13.1 \text{ Gyr}$ ). We will refer to them as the cosmology and the classical cosmology respectively.

## 2 THE FUNDAMENTAL PLANE OF EARLY-TYPE GALAXIES

Early-type galaxies are a rather homogeneous family of galaxies. It has been early on recognized that several observables, describing their dynamical state, size, and chemical composition, correlate with luminosity. Typical examples are the effective radius ( $R_e$ ; Fish 1964), the central velocity dispersion ( $\sigma$ ; Faber & Jackson 1976), the effective surface brightness ( $SB_e$ ; Binggeli, Sandage & Tarenghi 1984), the integrated colours (Bower, Lucey & Ellis 1992 and references therein), and metal indices such as  $M_{\text{g}_2}$  (Bender, Burstein & Faber 1993 and references therein).

The relatively large scatter of these correlations suggests that a ‘second parameter’ could be involved. The ‘second parameter’ was found when large spectrophotometric surveys during the mid-eighties revealed the existence of a tight relation between effective radius, effective surface brightness, and central velocity dispersion (Djorgovski & Davis 1987; Dressler et al. 1987). The relation,

$$\log R_e = \log \sigma + SB_e + \text{const}; \quad (1)$$

where  $R_e$  is in kpc (we will reserve the notation  $r_e$  when such radius is measured in arcsec),  $\sigma$  in  $\text{km s}^{-1}$ , and  $SB_e$  in  $\text{mag arcsec}^{-2}$ , was called the Fundamental Plane (FP). Because the value of the Hubble constant enters the relation through the calculation of the effective radius in kpc, the value of  $\text{const}$  depends on  $H_0$ . In the following we will call FP-space the three-dimensional space defined by  $\log R_e$ ,  $\log \sigma$ , and  $SB_e$ .

The quantities  $SB_e$  and  $R_e$  are found to depend on the wavelength of observation, as a result of colours and colour gradients in the stellar populations of early-type galaxies. When needed, we will explicitly state the dependence on

wavelength by adding a subscript (e.g.,  $R_{eB}$  is the effective radius in the B band). Not much is known about systematic variations of  $\text{const}$  with the spectral range used for the measurements. In P II we showed that no significant variation is noticed if lines such as Ca H and K or Na D are included or excluded from the spectral region of the measurement. In the following, in order to compare our data to data from the literature, we will assume that the value of the central velocity dispersion does not depend on the spectral region used for the measurement.

The intercept depends on wavelength. For example, in the Coma Cluster, Bender et al. (1998) report in the B band  $\text{const} = 8.895$  assuming  $h_{50} = 1$ ; in the V band, using the sample and slopes of Lucey et al. (1991),  $\text{const} = 8.71$  is found. The determination of  $\text{const}$  is hampered by the errors in the determination of distances and extinction. No differences, within the observational errors, have been found among the intercepts (and slopes) of the FP of nearby clusters and the field (Pahre, de Carvalho & Djorgovski 1998).

The slope is very well determined, independently of the different selection criteria and fitting techniques adopted by various groups; in addition, it does not change significantly with wavelength (Pahre, Djorgovski & de Carvalho 1998; Scodeggio et al. 1998). A typical value is  $\text{slope} = 0.32$ . The slope suffers from larger uncertainties and it is observed to vary with wavelength (Pahre et al. 1998b; Scodeggio et al. 1998). Accurate measurements over large samples of galaxies have shown that the observed scatter of the FP is larger than the observational errors (e.g. Jorgensen, Franx & Kjaergaard 1996). In other words, a significant fraction ( $0.07$ – $0.08$  in  $\log R_e$ ) of the observed scatter is due to scatter in the physical properties of E/S0. Within the observational errors, the intrinsic scatter is observed to be constant with wavelength and along the FP.

### 2.1 The physical origin of the FP

The very existence of the FP is a remarkable fact. Any theory of galaxy formation and evolution must be able to account for its tightness and its universality. In the following we will address the issues of how the observables entering the FP may be related to intrinsic physical quantities such as mass and luminosity of early-type galaxies and we will list some of the physical processes that have been proposed to be at the basis of the FP. In addition we will describe how the existence of the FP and its tightness can be used to derive information on the formation and evolution of early-type galaxies.

Let us define an effective mass  $M$ ,

$$M = \frac{2}{G} R_e \sigma^2; \quad (2)$$

where  $G$  is the gravitational constant. If homology holds, i.e. early-type galaxies are structurally similar, the total mass  $M$  (including dark matter if present) is proportional to  $M$

$$M = c_1 M \quad (3)$$

and we can interpret Eq. 2 in terms of the Virial Theorem. If  $c_1$  depends on mass, then we will say that weak homology holds.

Let us also define the effective luminosity  $L$  as

$$2.5 \log L = SB_e - 5 \log R_e - 2.5 \log 2; \quad (4)$$

In general, from the FP and Equations 2 and 4 we have:

$$L / 10^{2.5} M^{-\frac{10}{5}} R_e^{-\frac{2}{5}} : \quad (5)$$

The observed values for 10 cluster around to zero, although there is significant scatter that could be related to differences in the selection of the samples, in the determination of distances, in the fitting techniques, and extinction corrections. If

$$10^{-2} = 0; \quad (6)$$

then Equation 5 can be reduced to a power law relation between effective mass and luminosity (e.g. Faber et al. 1987; van Albada, Bertin & Stiavelli 1995):

$$L / M ; \quad (7)$$

where

$$= 0.2 : \quad (8)$$

Based on these definitions, the  $M=L$  (effective mass-to-light ratio) of a galaxy is readily obtained in terms of the FP observables:

$$M=L / 10^{0.45 B} e^{-2} R_e^{-1} : \quad (9)$$

By comparing  $M=L$  to the value predicted by the FP for the same effective radius and velocity dispersion,

$$(M=L)_{FP} / 10^{-2.5} M^{\frac{10}{5}} R_e^{-\frac{2}{5}} ; \quad (10)$$

the scatter of the FP can be connected to the scatter in  $M=L$  of the early-type galaxy population:

$$i \log(M=L^i) - \log(M=L)_{FP}^i = \frac{i}{(2.5)^2} \quad (11)$$

where the superscript  $i$  labels the galaxies of the sample under consideration, and  $i$  is defined as

$$i = \log R_e^i - \log i - SB_e^i : \quad (12)$$

Thus, the remarkable tightness of the FP implies a very low scatter in the  $M=L$  of early-type galaxies.

When a theoretical effort to understand this empirical scaling law is made, it is necessary to model the relation between effective mass and total mass ( $M$ ) and the relation between stellar ( $M$ ) and total mass. For example, if we assume

$$M / M / M ; \quad (13)$$

then Equations 2 and 10 yield

$$\frac{M}{L} / 10^{-2.5} M^{\frac{5}{5}} R_e^{-\frac{10}{5}} : \quad (14)$$

By neglecting their mild dependence on effective radius, Equation 14 implies that the stellar mass-to-light ratio depends on the total mass of the galaxy. This phenomenon is sometimes referred to as the tilt of the FP (Renzini & Ciotti 1993; see also Bender, Burstein & Faber 1992; Pahre et al. 1998b).

Several interpretations in terms of properties of the stellar populations have been suggested to explain the tilt of the FP (see, e.g., Renzini & Ciotti 1993; Ciotti, Lanzoni & Renzini 1996; Graham & Colless 1997; Pahre et al. 1998b). However no conclusive interpretation of the FP has been found

so far. Some of the hypotheses have turned out to be insufficient to explain the FP (e.g. the tilt cannot be attributed entirely to a relation between metallicity and mass, Pahre et al. 1998b). On the other hand, the viable hypotheses require an ‘unnatural’ fine tuning in order to explain the tilt while preserving the tightness.

The remarkable tightness of the FP can be used to set constraints on the formation and evolution of early-type galaxies. For example, assuming weak homology and a proportionality between total mass and stellar mass, we know from the FP that at any given mass the scatter in  $\log(M=L)$  is very small ( $< 0.10$ ). If we attribute such scatter entirely to scatter in age, we can set an upper limit to it ( $\propto t^{-1}$ ). Similarly, we can set an upper limit to the scatter in metallicity ( $\propto Z$ ). Unfortunately, correlations between the various effects can conspire to keep the scatter small, so that, for example, a small scatter in  $\log(M=L)$  does not necessarily imply a small scatter in both age and metallicity.

The absence of a difference between the FP of field and cluster E/S0 is also a remarkable fact. For example, within the scheme described in this section, it can be interpreted in terms of the absence of significant differences between the average  $M=L$ , and thus between the stellar populations, of field and cluster E/S0. This fact is consistent with the very small difference found between the  $M-g$  relation (in which the observables are distance independent) of a large sample of local ellipticals in the cluster and in the field environments by Bernardi et al. (1998).

A very effective way to further investigate the origin of the FP, and thus to learn about the evolution of E/S0, is to study the FP as a function of redshift. In fact, with this information it is possible to distinguish between models that predict an evolution of the slopes with redshift, e.g. the model where the tilt is due to Initial Mass Function (IMF) effects (see Renzini & Ciotti 1993), and models that do not, e.g. the model where the tilt is due to dark matter distribution. Similarly for the scatter: if the scatter is due to scatter in the ages of the stellar populations, then it should increase with look-back time; if it is due to scatter in metallicity, it should not.

## 2.2 The FP at intermediate redshift as a diagnostic of the evolution of stellar populations

Recently it has been observed that early-type galaxies in clusters at intermediate redshift also populate a tight FP (van Dokkum & Franx 1996; Kelson et al. 1997; van Dokkum et al. 1998b; Bender et al. 1998; Pahre 1998; Jorgensen et al. 1999; Kelson et al. 2000b).

The intercept of the FP ( $\alpha$ ) is observed to vary as a function of redshift. So far, no dramatic change in the slopes with redshift has been reported, even though an accurate measurement is difficult, because of the small samples available and of the intrinsic problems in this measurement, such as completeness corrections and fitting technique (see, e.g., van Dokkum & Franx 1996; T99; Jorgensen et al. 1999, Kelson et al. 2000b). For example, Kelson et al. (2000b), using the largest sample at intermediate redshift ( $z = 0.33$ ) published at the moment of this writing (30 E/S0 galaxies in a single cluster), find  $\alpha = 1.31 \pm 0.13$  and  $\alpha = 0.344 \pm 0.10$  in the V band; these values are indistinguishable from those found

locally. The absence of a dramatic change in the slopes argues against the interpretation of the FP solely in terms of an age-mass relation.

A simple explanation of these findings can be given by recalling the correspondence of the FP observables to  $M$  and  $M = L$ . Let us consider a sample of galaxies with observables labelled by superscript  $i$ . Let us assume that effective radius and central velocity dispersion do not change on the observed time-scale. For each galaxy, we can compute the variation of the logarithm of the effective mass-to-light ratio with redshift,

$$\log(M = L)^i - \log(M = L)_{z=z_2}^i = \log(M = L)_{z=z_1}^i; \quad (15)$$

in terms of the variation of combinations of the coefficients of the FP with  $z$  from Eq. 10:

$$\log(M = L)^i = \frac{10 - 2}{5} \log \alpha^i + \frac{2.5}{5} \log R_e - \frac{i}{2.5}; \quad (16)$$

where the symbol  $\Delta$  indicates the difference of the quantity at two redshifts as in Equation 15.

For the analysis presented here we will assume that  $\alpha$  and  $R_e$  are constant. This assumption is broadly consistent with the observations and makes the interpretation of the results straightforward. In fact, if  $\alpha$  and  $R_e$  are constant, we have that:

$$\log(M = L)^i = \frac{i}{2.5}; \quad (17)$$

i.e. the evolution of  $\log(M = L)^i$  depends only on the evolution of  $i$ . In practice, by measuring  $i$  for a sample of  $N_g$  galaxies at intermediate redshift, and by comparing it to the value of the intercept found in the local Universe ( $i_0$ ), we can measure the average evolution of  $\log(M = L)$  with cosmic time:

$$\langle \log(M = L) \rangle = \frac{i_0 - N_g}{2.5 N_g}; \quad (18)$$

i.e., if the intercept  $i_0$  is computed as the average of  $i$ ,

$$\langle \log(M = L) \rangle = \frac{i_0}{2.5}; \quad (19)$$

Similarly, the intrinsic scatter of  $M = L$  is related to observable quantities by Equation 11, and therefore its evolution with redshift can be measured. Note that, by assuming constant  $R_e$  and  $\alpha$ , we are neglecting any structural and dynamical evolution of the galaxies; in addition, by assuming constant  $\alpha$  and  $R_e$ , we obtain that the evolution of  $M = L$  is independent of  $M$ .

In the spirit of this observational study, we will focus our attention on the measurement of the evolution of the effective mass-to-light ratio  $M = L$  and we will not attempt to address the issues associated with the relation between the effective mass  $M$  and the total mass  $M_{\text{tot}}$ . In particular, we will limit our study to the evolution of stellar populations, neglecting any dynamical or structural evolution. In other words, the only properties of the galaxies that will be allowed to vary in our study will be those of the integrated stellar population. The comparison with the expectations of passive evolution models will be done by assuming that:

$$M_{\text{tot}} / M = \text{constant}; \quad (20)$$

Two effects must be kept in mind when applying this diagnostic:

(i) Morphological evolution. If galaxy types evolve into one another, then locally-type galaxies are not simply the evolution of intermediate redshift ones. For example, if spirals evolve into early-type galaxies as suggested by hierarchical clustering scenarios, then the FP at intermediate redshift can look tight and slowly evolving because E/S0 are being recognized only when their stellar populations are already old.

(ii) Cluster population evolution. The population of galaxies within clusters is likely to evolve with redshift. If this happens, then the comparison of cluster and field samples can be biased.

A complete analysis of these effects requires a comprehensive theoretical model, able to describe the joint evolution of galaxies and of their environment. Such modeling is beyond the aims of this observational study. Therefore, we will mostly limit our presentation to the observational results (to be used as a constraint when testing models). In order to facilitate comparison with theoretical models, the sample selection process has been defined as clearly as possible in Part II. Some considerations on the population biases in the context of simple passive evolution of the stellar populations are presented in Section 6.5.

The comparison of the stellar populations in cluster and field environment is particularly interesting. In fact, as mentioned in the Introduction, one of the expectations of hierarchical clustering models is that early-type galaxies and their stellar populations form much later in the field than in the core of rich clusters. Unfortunately, in the local Universe, in addition to the observational uncertainties listed in Section 2, the detection of a possible difference between cluster and field galaxies with the FP is hampered by the generally old age of their stellar populations. It is easier to detect any possible difference at intermediate redshift, where the FP is in principle more sensitive. In fact, since peculiar velocities (the motion with respect to the local comoving system) are limited (a few hundreds of  $\text{km s}^{-1}$ , see e.g. Groth, Juszkiewicz & Ostriker 1989), the uncertainty on distance determination becomes negligibly small with increasing redshift. In addition, if the stellar populations of field and cluster E/S0 had different average ages, any difference in the FP should increase with redshift thus becoming detectable.

### 2.3 The $SB_e$ - $R_e$ relation

The correlation associated with the projection of the FP on the photometric plane, also known as the  $SB_e$ - $R_e$  relation (Komberg 1977),

$$SB_e = a_1 \log R_e + a_2 \quad (21)$$

is very useful for our purposes because it does not involve internal kinematics. Therefore, it can be followed to higher redshifts and fainter absolute magnitudes. The drawback is that the  $SB_e$ - $R_e$  relation has a larger intrinsic scatter than the FP and its coefficients are much more sensitive to sample selection biases (see, e.g., Capaccioli, Cea & D'Onofrio 1992). In the following we will use the evolution of the  $SB_e$ -

Re relation to extend the findings achieved with the FP to higher redshift and to fainter absolute luminosities.

### 3 THE DATA

The galaxies have been selected on the basis of HST-WFPC2 images taken from the HST-Medium Deep Survey (Gri ths et al. 1994), mainly based on colour, magnitude, and morphology. The sample selection criteria are extensively discussed in P II and are taken into account in the analysis presented here. Briefly, we can say that the sample analyzed in this paper is representative of the population of early-type galaxies at  $z = 0.1 - 0.5$  with  $0.95 < V_{606} - I_{814} < 1.7$  and  $I_{814} < 19.3$  (as in P II  $V_{606}$  and  $I_{814}$  indicate Vega magnitudes through HST filters F606W and F814W respectively).

The sample is a field sample in the sense that the galaxies are selected on random WFPC2 pointings, excluding the regions of known clusters. On the basis of the images available, it is not possible to identify and to exclude members of groups or galaxies in the outskirts of rich clusters. In this respect, our operational definition of field does not coincide with the definition used in theoretical investigations, where the full three dimensional and dynamical information available is used to identify rich clusters, groups, and field (e.g., Kaumann 1996).

The data, the data reduction, and the caveats of the photometric and spectroscopic measurements are described in P II. For quick reference, we summarise in Table 1 the relevant observed quantities for the sample of E/S0 analyzed in this paper.

### 4 OBSERVATIONAL RESULTS

In this section we will discuss the location of our sample of field early-type galaxies at intermediate redshift in the FP-space in comparison to the location of local samples. Only galaxies that obey the selection criteria listed in P II are considered.

In principle, one would like to compare the intermediate redshift data to field local data. However, as discussed in Section 2, no significant difference has been found so far in the local Universe between the FP in the field and that in the cluster environment, within the accuracy allowed by the uncertainties in the determination of distances, reddening corrections, and the small size of the available samples (Pahre et al. 1998a). For these reasons, we will compare the intermediate redshift data to the FP of the Coma cluster, a well defined relation, with selection biases under control.

The discussion will be extended to a larger sample of galaxies in Section 4.2 by means of the projection of the FP on the photometric plane, the  $SB_e$ - $R_e$  relation, including galaxies without measured velocity dispersion.

#### 4.1 The Fundamental Plane of field early-type galaxies at intermediate redshift

In Figures 1 to 4, panels (a), (b), and (c), we plot the location in the FP-space of the intermediate redshift galaxies binned in redshift. The data are shown in the rest-frame B and V bands and for two choices of values for the cosmological

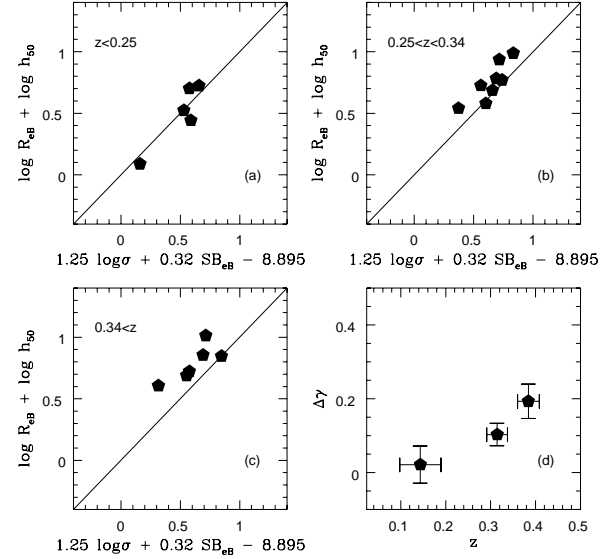


Figure 1. Fundamental Plane in the rest-frame B band at intermediate redshift. In panels (a), (b), and (c) we plot the intermediate redshift galaxies (pentagons) binned in redshift. The solid line represents the FP of Coma, as measured by Bender et al. (1998). In panel (d) the average offset of the intercept (at fixed slopes  $\alpha$  and  $\beta$ , taken from Bender et al. 1998) is plotted as a function of redshift. The error bars are the standard deviation of the mean. The classical cosmology is assumed.

parameters (see captions). Since errors on the photometric parameters are correlated, we do not show them in this projection. A better visualization of the errors is given in the projection that separates kinematics and photometry, used in Figures 5 and 6. In panels (d) of Figures 1 to 4 we show the evolution of the intercept of the FP with redshift.

Qualitatively, two main facts emerge:

(i) Existence of the FP. At any given redshift between  $z = 0$  and  $z = 0.4$  the FP of field early-type galaxies is well defined. The scatter is small. No trend of increasing scatter with redshift is noticeable within the accuracy allowed by the small number statistics available.

(ii) Evolution of the FP. At given  $R_e$  and  $\sigma$ , the intermediate redshift galaxies have brighter effective surface brightness with respect to the values predicted by the local relation (solid line) and hence are more luminous and have lower  $M = L$ . The average offset increases with redshift, as shown in panels (d).

To make these statements more quantitative, let us describe the evolution of the intercept (at fixed slopes  $\alpha$  and  $\beta$ ) with a linear relation:

$$\Delta\gamma = \gamma_0 + \gamma_1 z \quad (22)$$

With a least squares fit (see Figure 7) applied to the data in the V band we obtain  $\gamma_0 = 0.44 \pm 0.03$  (classical cosmology) and  $\gamma_1 = 0.56 \pm 0.04$  (cosmology); in the B band we obtain  $\gamma_0 = 0.45 \pm 0.04$  (classical cosmology) and  $\gamma_1 = 0.57 \pm 0.04$  (cosmology). This description allows us to estimate the scatter of the FP in any redshift bin. In fact, there are three contributions to the scatter: the measurement error, the intrinsic scatter, and the evolutionary drift. The last item is

Table 1. Summary of observed quantities. For each galaxy (gal) we list redshift, central velocity dispersion ( $\sigma$ , if measured; in  $\text{km s}^{-1}$ ), effective radius ( $r_e$ ; in arcsec), and effective surface brightness ( $SB_e$ ; in  $\text{mag arcsec}^{-2}$ ) in the rest-frame B and V bands. Details on the measurements are given in P II. Note that the errors on the effective radius and the effective surface brightness are correlated: the combination that enters the FP,  $r_e SB_e$ , is better determined than the individual quantities (for a discussion see P II; see also Figures 5 and 6).

gal	z			$r_{eB}$		$SB_{eB}$		$r_{eV}$		$SB_{eV}$	
A 1	0.147	242	24	1.59	0.14	20.54	0.08	1.64	0.07	19.67	0.13
D 1	0.385	309	28	0.78	0.10	19.80	0.20	0.70	0.07	18.77	0.16
E 1	0.294	211	28	0.89	0.09	20.78	0.15	0.93	0.08	19.91	0.21
F 1	0.295	–		1.11	0.00	21.53	0.07	1.05	0.00	20.55	0.09
G 1	0.295	234	22	1.59	0.22	20.78	0.20	1.51	0.12	19.80	0.18
I 1	0.293	202	23	0.64	0.12	19.96	0.26	0.64	0.07	19.06	0.24
C 2	0.425	–		1.04	0.10	20.21	0.16	1.00	0.09	19.42	0.12
D 2	0.192	–		0.37	0.32	18.68	0.96	0.40	0.17	18.08	0.74
E 2	0.398	233	16	1.61	0.08	20.78	0.09	1.48	0.08	19.77	0.10
F 2	0.336	252	23	1.00	0.09	20.73	0.14	0.94	0.05	19.74	0.11
A 3	0.231	201	18	1.08	0.13	20.60	0.14	0.97	0.07	19.42	0.14
B 3	0.490	–		0.23	0.01	17.57	0.18	0.23	0.03	16.98	0.31
C 3	0.106	155	19	0.48	0.08	19.74	0.14	0.47	0.05	18.78	0.10
E 3	0.263	–		1.31	0.16	21.70	0.12	1.30	0.10	20.87	0.16
G 3	0.408	259	17	0.81	0.16	20.17	0.36	0.77	0.17	19.19	0.40
I 3	0.410	207	16	0.62	0.11	19.74	0.28	0.65	0.10	18.93	0.23
M 3	0.337	243	19	0.90	0.13	20.23	0.18	0.83	0.08	19.25	0.13
R 3	0.348	243	15	1.20	0.09	20.64	0.12	1.16	0.11	19.71	0.21
S 3	0.356	230	23	1.16	0.11	21.22	0.29	0.86	0.05	19.60	0.07
T 3	0.117	142	30	1.18	0.14	21.05	0.20	1.27	0.08	20.29	0.08
A 4	0.117	178	19	0.99	0.20	20.85	0.02	0.95	0.11	19.75	0.13
D 4	0.285	238	21	1.14	0.06	20.67	0.05	1.11	0.04	19.73	0.07
H 4	0.340	231	16	1.65	0.12	21.17	0.10	1.58	0.06	20.25	0.10
I 4	0.337	258	27	0.65	0.17	20.26	0.38	0.65	0.09	19.43	0.24
B 4	0.211	–		0.54	0.03	20.43	0.06	0.62	0.02	20.06	0.03

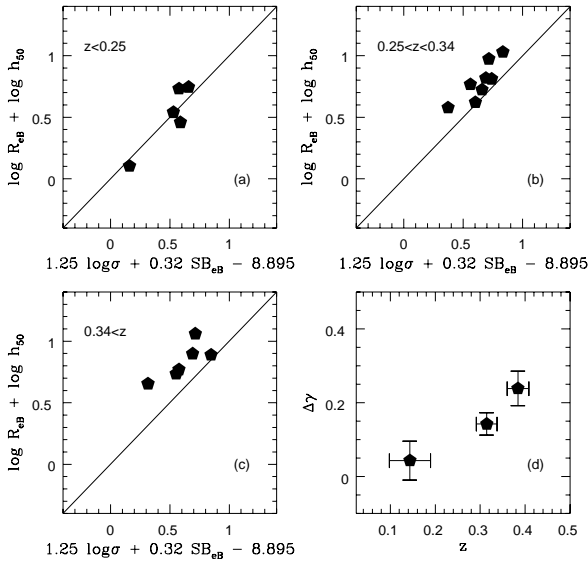


Figure 2. As in Figure 1, in the cosmology.

simply the combined effect of the width of the redshift bins and the evolution of the intercept. We can correct for the scatter induced by the evolutionary drift by ‘evolving’ the galaxies to the average redshift of the bin with Equation 22. The corrected scatter thus obtained is remarkably small and constant with redshift (0.08–0.09 in  $\Delta\gamma$ ). In Figure 7 we plot

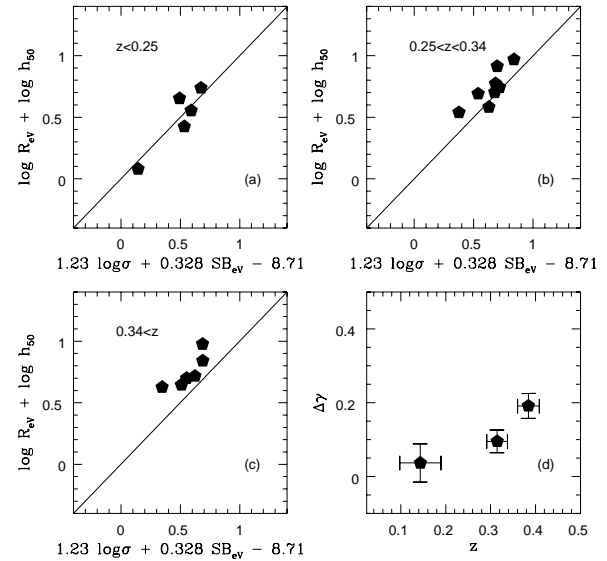


Figure 3. As in Figure 1 (classical cosmology), data in the rest-frame V band. The FP of Coma, drawn as a solid line, is taken from Lucey et al. (1991).

the evolution of the intercept with redshift together with the best-fitting line. The thin error bars represent the total scatter, while the thick error bars represent the scatter corrected for evolution. It is harder to separate the contribution

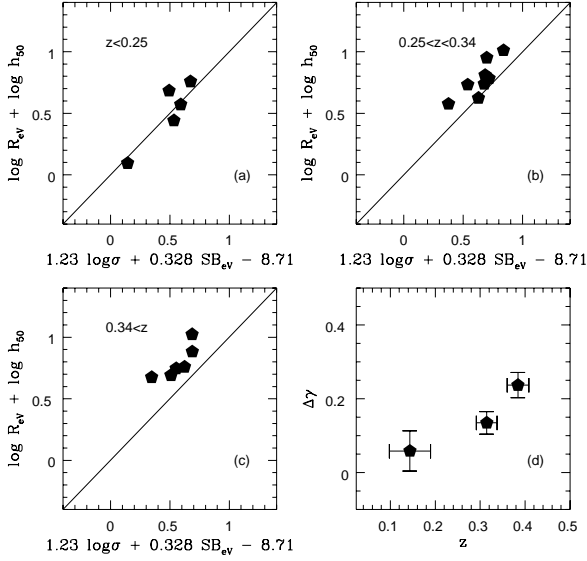


Figure 4. As in Figure 3, in the cosmology.

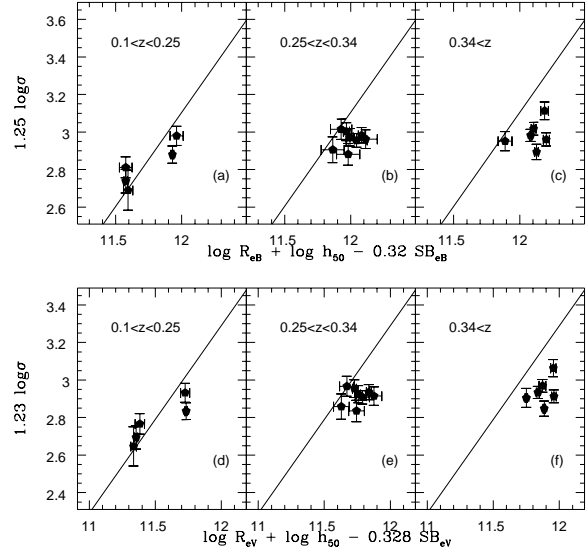


Figure 6. As in Figure 5, in the cosmology.

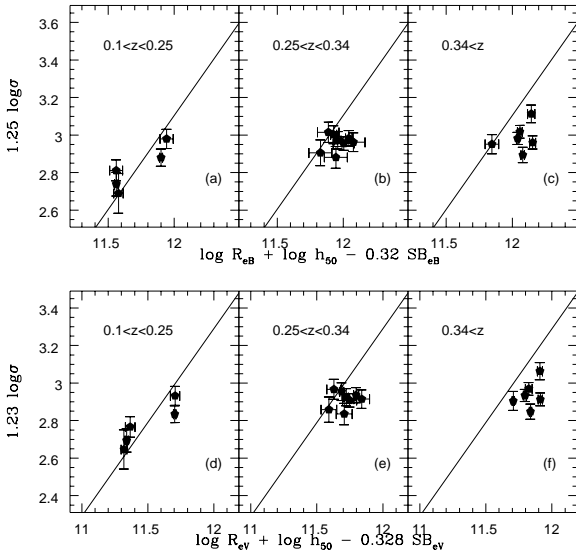


Figure 5. Evolution of the FP in the B (upper panels) and V bands (lower panels), in the classical cosmology. The symbols are as in Fig 1. The Fundamental Plane is seen here in the projection most natural for the description of errors, with photometric and kinematic measurements on different axes. The errors on the photometric parameters are correlated; the combination that enters the FP is particularly robust (see P III).

from measurement errors, because they are correlated and include a systematic component. However, by subtracting in quadrature the average uncertainty on  $\sigma$  (for a single galaxy this is 0.05–0.06) one can estimate the intrinsic scatter to be approximately 0.05–0.07. Given the limited number of galaxies available per redshift bin, the error on the scatter is quite large ( $\sim 30$  per cent for a Gaussian distribution, neglecting systematics). Nevertheless, a substantial increase

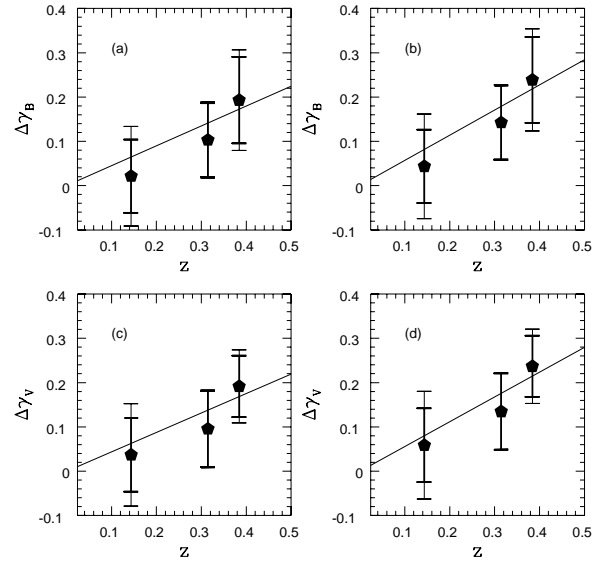


Figure 7. Evolution of the intercept of the FP and its scatter with redshift. The solid line is a least-squares linear fit to the data. The thin error bars are the measured scatter, the thick error bars are the scatter corrected for its evolutionary component (see Section 4.1). The classical cosmology is used in panels (a) and (c), the cosmology in panels (b) and (d).

in the scatter can be ruled out. Larger samples are needed in order to measure the scatter as a function of redshift accurately.

#### 4.2 The $SB_e$ - $R_e$ relation at intermediate redshift

We will now study the evolution of the  $SB_e$ - $R_e$  introduced in Section 2.3 on the larger sample available without internal kinematic information. The sample includes 25 galaxies



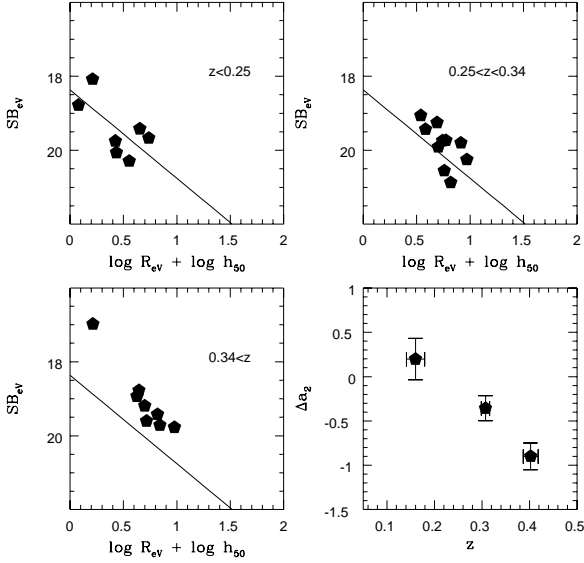


Figure 8.  $SB_e-R_e$  relation for field early-type galaxies at intermediate redshift in the V band. The solid line is the best fit to the Coma data by Lucey et al. (1991). The classical cosmology has been used to derive effective radii. The average offset is plotted in panel (d) as a function of redshift. Error bars are the standard deviation of the mean of the sample.

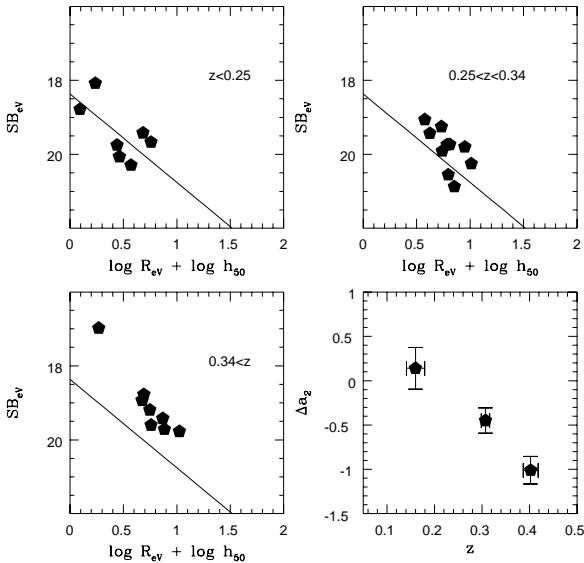


Figure 9. As in Figure 8, in the B cosmology.

out to  $z = 0.49$ . The results in the V band are plotted in Figures 8 and 9. The results in the B band are very similar (see figures in Section 6).

Following the analysis of the previous section, we describe the evolution of the intercept of the  $SB_e-R_e$  relation ( $a_2$  of Equation 21) with a linear relation,

$$a_2 = a_2^0 + \alpha_2 z. \quad (23)$$

By means of a least squares fit, we find  $a_2^0 = 1.30$  (classical

cosmology) and  $a_2^0 = 1.59$  (B cosmology) in the V band. In the B band we find  $1.37$  and  $1.67$  respectively.

In the context of passive evolution of stellar populations, with the assumption that the stellar mass is proportional to the effective mass  $M_{\text{eff}}/M$ , Equations 19 and 22 yield:

$$\langle \log(M_{\text{eff}}/M) \rangle = \frac{z}{2.5}. \quad (24)$$

Thus, if we assume that  $R_e$  and  $a_1$  (Equation 21) are constant with redshift, and that the evolution of the  $SB_e-R_e$  relation is given by passive evolution of  $M_{\text{eff}}/M$ , i.e.

$$a_2 = SB_e = 2.5 \langle \log(M_{\text{eff}}/M) \rangle; \quad (25)$$

$a_2^0$  should be related to  $a_1^0$  by:

$$a_1^0 = a_2^0. \quad (26)$$

The values found for  $a_1^0$  and  $a_2^0$  are in excellent agreement with this relation. Naturally, the agreement does not prove that either result is correct, since the comparison depends on rather strong assumptions. Nevertheless, this provides an obvious consistency check for both the observations (that rely on independent local relations) and the pure passive evolution interpretation.

## 5 SELECTION EFFECTS

For a physical interpretation of the results it is crucial to have a full control of the relevant selection effects. In particular, from the point of view of the evolution of stellar populations it is important to quantify the effects of the colour selection and the magnitude limit. As described in P II, we selected our galaxies from the MDS catalog<sup>?</sup>, according to  $I_{814} < 19.3$  and  $0.95 < V_{606} - I_{814} < 1.7$ . In Figure 10 we plot magnitudes and colours of the galaxies in the observed sample, together with the selection criteria represented by solid lines.

Two main potential biases can be introduced by our selection. On the one hand, at high redshift ( $z > 0.4$ ), the typical luminosity approaches that of the selection criterion in  $I_{814}$ . On the other hand, at low redshift ( $z = 0.1 - 0.2$ ), the colours of the galaxies in our sample approach the lower limit in the selection criterion. In this section we will focus mostly on the former potential bias, while the latter will be better addressed in the next section, with the help of evolutionary population synthesis models.

Some examples clarify these selection effects. Let us first consider a toy population of galaxies with the following properties. For given  $a_1$  and  $R_e$ , the scatter in  $SB_e$  results from measurement errors and the intrinsic scatter of the FP; the colour is not correlated with the offset of the intercept. For this toy population, the magnitude limit will tend to select the brightest objects, thus simulating a stronger evolution of the intercept of the FP. The magnitude of the bias depends on the measurement error and the intrinsic scatter of the FP.

<sup>?</sup> By comparing our photometry with that of the MDS group we find an average difference of less than 0.01 both in colour and  $I_{814}$  magnitude and an r.m.s. scatter of 0.11 and 0.12 respectively in colour and  $I_{814}$  magnitude. The scatter is taken into account in the treatment of the selection effects.

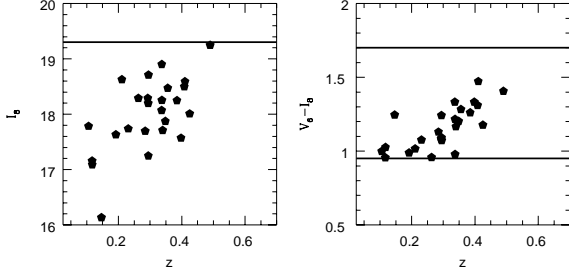


Figure 10. Left panel: observed  $I_{814}$  magnitude, as measured by the MDS group, as a function of redshift. The limit for sample selection ( $I_{814} < 19.3$ ) is plotted as horizontal line. Right panel: observed  $V_{606}-I_{814}$  colour, as measured by the MDS group, as a function of redshift. The limits for sample selection ( $0.95 < V_{606} - I_{814} < 1.7$ ) are plotted as horizontal lines.

This effect can be quantified as follows. Let us assume that at  $z = 0.4$  (the highest redshift, where the effect is stronger) field early-type galaxies define an FP with slopes and equal to those of Coma. The built-in intercept is offset by  $\Delta\gamma_{th}$  with respect to the FP of Coma, and the scatter is kept as a parameter. A population of galaxies is created by a routine implementing a Monte Carlo algorithm, the magnitude limit  $I_{814} < 19.3$  applied, and the observed  $\gamma_{obs}$  recovered. This is repeated for a range of values of  $\Delta\gamma_{th}$ .

In Figure 11, panel (a), we plot the ratio  $\gamma_{obs}/\gamma_{th}$  as a function of  $\gamma_{obs}$  and for various values of the intrinsic scatter. As expected, the bias is important for low values of  $\gamma_{obs}$  and for high values of the scatter. For our observed values ( $\gamma_{obs} = 0.2$ – $0.25$ , scatter  $0.08$ ) the effect is small ( $< 5$  per cent). In addition, we can use the same simulation to check whether the selection effects introduce any bias in the determination of the scatter. In panel (b) we plot the ratio of the recovered scatter ( $\sigma_{obs}$ ) to the input scatter ( $\sigma_{th}$ ) as a function of  $\gamma_{obs}$ . For  $\gamma_{obs} = 0.2$ – $0.25$  the systematic effect is much smaller ( $< 10$  per cent) than the random error.

In a more realistic second example, let us consider a population of early-type galaxies with fixed metallicity and a broad distribution of ages. At  $z = 0.4$  our magnitude limit would tend to select the brightest (i.e. the youngest and bluest) objects. At  $z = 0.1$ – $0.2$ , the colour selection criterion will pick the reddest (i.e. the oldest and faintest) objects. In this case the colour and magnitude selection effects are connected, and some modeling of the evolution of the galactic spectra is required to study the bias. The next section reports a quantitative analysis of these problems based on a Bayesian-Monte Carlo approach.

## 6 CONSTRAINTS ON THE EVOLUTION OF STELLAR POPULATIONS

In this section we analyse the results presented above in terms of passive evolution of the stellar populations. First, in 6.1, we compare the data to the prediction of single-burst passive evolution models based on Bruzual & Charlot (1993; G1SSEL96 version, hereafter BC96) synthetic spectra. In this first qualitative analysis selection biases are ne-

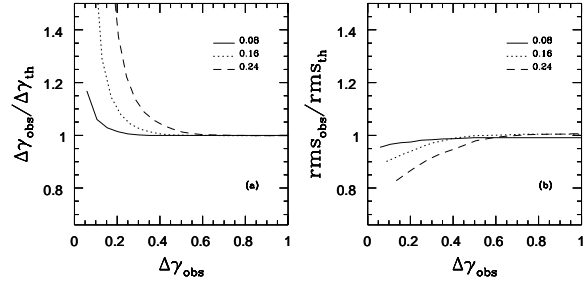


Figure 11. Estimate of the magnitude selection bias. Panel (a): due to the magnitude limit (see Fig. 10) the value of  $\gamma_{rec}$  recovered from observation ( $\gamma_{obs}$ ) can be higher than the input value ( $\gamma_{th}$ ); here we plot the ratio of the observed to input value as a function of observed value. Panel (b): The magnitude limit can also bias the observed scatter ( $\sigma_{obs}$ ); here we plot the ratio of the observed scatter to the input scatter ( $\sigma_{th}$ ). The curves are derived with Monte Carlo simulations at  $z = 0.4$ , i.e. the highest redshift bin, where the effects are stronger. The curves are labelled with the intrinsic scatter in  $\gamma$  of the FP. The cosmology is assumed. Similar results are obtained for the classical cosmology.

glected. In the following Section 6.2 we introduce a Bayesian-Monte Carlo approach (see below and the description of the algorithm in Treu 2001), useful to derive quantitative results, taking into account the selection process. In its simplest version, the approach is used to calculate the a posteriori probability density (i.e. the probability density given the present set of observations) of the parameter defined in Equation 22. Then the Bayesian-Monte Carlo approach is combined with the BC96 spectral synthesis models to derive constraints on the star formation history of the galaxies in the sample.

As is well known, the problem of determining the star formation history of stellar populations from the Fundamental Plane (and the SBE-Re relation) is sensitive to the value of the cosmological parameters and the modeling of the stellar populations. In particular, it depends on the choice of the Initial Mass Function (IMF; see Schade et al. 1997). For this reason, the evolution of the FP can be used to constrain the cosmological parameters and/or the IMF (Bender et al. 1998; van Dokkum et al. 1998b). In the present study, in order to limit this sort of degeneracies, we focus on the ‘best-guess’ for the value of the cosmological parameters and the form of the IMF (cosmology and Salpeter IMF) and then we try to extract the maximal information on the star formation history. In order to give an idea of what is robust and what is sensitive to the assumptions about the cosmological parameters and the IMF, we will also present the results for the classical cosmology and for the  $\text{ScalD IMF}$ . For completeness we briefly discuss (Section 6.3) the limits that can be set on the cosmological parameters.

In Section 6.4 we discuss potential systematic biases and in Section 6.5 we extend the discussion of the population biases introduced in Section 2.2.

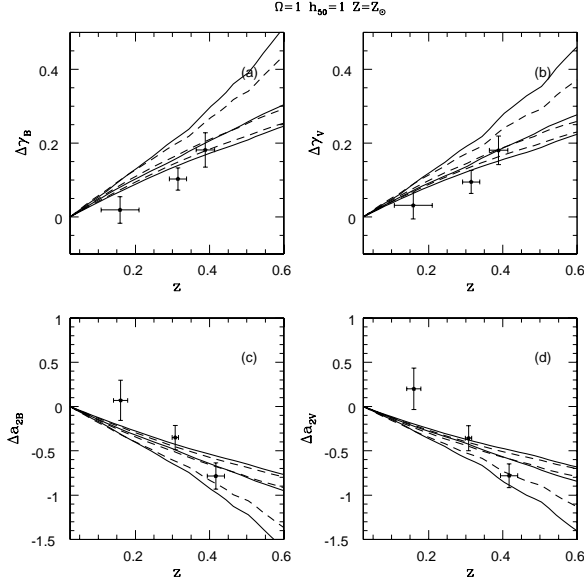


Figure 12. Single-burst passive evolution models. The evolution of the intercept of the FP is compared to the prediction of single-burst passive evolution models computed from BC96 synthetic spectra in panels (a) and (b). The comparison is repeated in panels (c) and (d) for the  $SBE-R_E$  relation, by including galaxies without measured velocity dispersion. The solid lines represent models with Salpeter IMF (Salpeter 1955), the dashed lines represent models with Scalo IMF (Scalo 1986). All models have solar metallicity. Three redshifts of formation are assumed,  $z_f = 1; 2; 5$ , from top to bottom in panels (a) and (b), from bottom to top in panels (c) and (d). The classical cosmology is assumed.

### 6.1 Single-burst models

In Figures 12 and 13 the evolution of  $\gamma$  and  $a_g$  as predicted by single-burst passive evolution models is shown and compared to the data. For each cosmological model we show the predictions obtained for single bursts occurred at  $z_f = 1; 2; 5$ . The results are shown for models with solar metallicity and K96 stellar atmospheres (see the documentation to BC96 for details). The results are highly insensitive to changes in metallicities and stellar atmospheres.

Qualitatively, we note that the data points are better reproduced by models with  $z_f > 2$  in the classical cosmology and with  $z_f = 1$  in the  $\Lambda$  cosmology.

### 6.2 A Bayesian-Monte Carlo approach to the evolution of stellar populations

We can better quantify the results obtained so far by means of a Bayesian-Monte Carlo approach. In the following we will give only a brief description of the method, which is outlined in detail elsewhere (Treu 2001).

#### 6.2.1 The evolution of the intercept of the FP

Let us assume that Equation 17 holds and that the intercept evolves as in Equation 22, i.e. linearly in redshift with slope  $(\gamma = z)$ . Under these assumptions we are able to calculate the probability  $p^i = p^i(\gamma^i)$  of observing a galaxy at redshift  $z^i$  with  $\gamma^i$  (defined as in Equation 12), where the

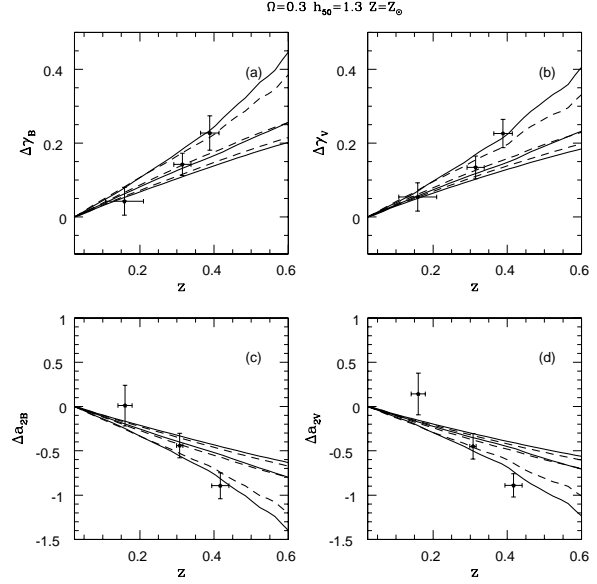


Figure 13. As in Figure 12, in the  $\Lambda$  cosmology.

superscript  $i$  indicates an individual galaxy within the set of observed galaxies. The probability density is obtained from Monte Carlo simulations (at least 1,000,000 random events per galaxy are generated, see Treu 2001), taking into account the intrinsic scatter of the FP (assumed to be constant with redshift as measured above), the observational errors, and the selection effects. Since galaxies are independent, the probability of observing the set  $f^i$  is:

$$p(f^i) = \prod_i p(\gamma^i) \quad (27)$$

We now apply Bayes Theorem (Bayes 1763; see also, e.g., Zellner 1971):

$$p(\gamma^i | f^i) = \frac{p(f^i | \gamma^i) p(\gamma^i)}{p(f^i) p(\gamma^i)} \quad (28)$$

to derive the probability of a value of  $\gamma$  given the set of measured  $f^i$  (the a posteriori probability, or simply the posterior). The probability density of  $\gamma$  prior to observations (the a priori probability, or simply the prior) can be used to take into account previous observations or physical limits. The choice of the a priori probability density in cases where investigators know little about the value of the parameter, or wish to proceed as if they knew little, is extensively discussed in the literature (see, e.g., Zellner 1971 and references therein; see also the recent review by Berger 1999). Traditionally, in the so-called Bayes-Laplace approach, a uniform prior was used. Alternative priors have been proposed, including some based on the requirement of invariance with respect to changes of parametrization (Jeffreys 1961) and others based on information arguments (see next paragraph; see also Zellner 1971). The advantage of the Bayesian approach is that it provides a probability distribution for the parameter (as compared for example to the confidence limits provided by a 'frequentist' approach), under well-controlled assumptions (such as the choice of the prior).

For simplicity, in the following we assume  $p(\gamma)$  constant within the interval  $(0.1; 1.5)$  and zero outside it, i.e.

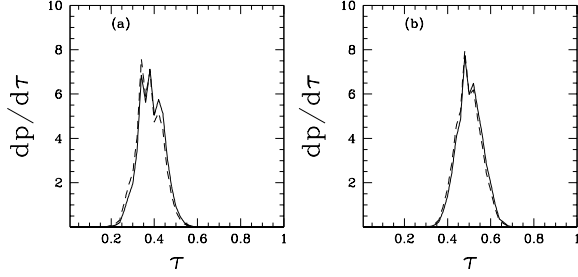


Figure 14. Evolution of the intercept of the FP in the V band. The a posteriori probability density of the slope of the relation  $\tau = z$  is shown here as recovered from a Bayesian-MonteCarlo approach that takes into account selection biases (see Section 6.2). The posteriors obtained with a uniform prior (solid line) and with a prior of the form  $p(\tau) \propto 1/\tau$  (dashed line) are shown. The results for the classical cosmology and the cosmology are shown in panels (a) and (b).

$$p(\tau) = 0.625H(1.5 - \tau)H(\tau + 0.1); \quad (29)$$

with  $H$  the Heaviside function, defined as  $H(x) = 1$  for  $x > 0$  and 0 otherwise. The interval has been chosen so as to include all the region where  $p(\tau) \neq 0$ . It is interesting to note that for a finite interval spanned by the parameter, the uniform prior is the proper (i.e. normalizable to 1) prior with minimal information (defined as  $-\int p(x) \log p(x) dx$ ; Zellner 1971). It is also noticed that for this choice of the prior the maximum of the posterior is the value that would be derived with a maximum likelihood algorithm.

The method described above, extended to the galaxies without measured velocity dispersion in terms of the SBE-Re relation as outlined by Treu (2001), gives the results shown in Figure 14 (V band). One significant limitation can be defined in the usual way, by requiring that the integral of the probability density over the interval be 0.68. In this way, we find  $0.33 < \tau < 0.44$  (classical cosmology) and  $0.44 < \tau < 0.56$  (cosmology). These intervals are consistent with the values found using a least  $\chi^2$  fit (see Equation 22 and the following discussion). However, the values found with the least  $\chi^2$  fit are on the higher end of the interval, not on the peak of the probability density (see Figure 14). We conclude that a correct treatment of the selection effects is important in order to derive reliable estimates.

In order to check that the results are robust with respect to the choice of the prior, we computed the posterior by assuming an alternative prior. For example, let us consider  $p(\tau) \propto 1/\tau$  (limited to  $\tau > 0$ ), which has the advantage that the results are unchanged under a power law change of parametrization  $X = \tau^n$  (see Zellner 1971 and references therein). In fact, by converting

$$p(X | \mathbf{f}^i g) / p(\mathbf{f}^i g | X) p(X) \propto \frac{p(\mathbf{f}^i g | X)}{X} \quad (30)$$

into a posterior in  $\tau$  we get

$$p^0(\tau | \mathbf{f}^i g) / p(\tau | \mathbf{f}^i g) \propto \frac{dX}{d\tau} \propto \frac{p(\mathbf{f}^i g | X)}{\tau^n}; \quad (31)$$

as is obtained by assuming  $p(\tau) \propto 1/\tau$ . The posterior obtained by taking this prior is shown in Figure 14 as a dashed

line; it is very similar to the one obtained by assuming a uniform prior (solid line).

## 6.2.2 Single-burst models

The Bayesian-MonteCarlo approach is used with the BC96 modeling of integrated stellar populations to obtain quantitative information on the star formation history of our sample of old early-type galaxies. Let us first consider a single population of galaxies with fixed IMF and stellar populations formed in a single-burst at  $z = z_f$  and evolving passively thereafter. Let us assume that in the local Universe such population obeys the FP relation of Coma. As usual, we will assume that the properties of the stellar populations are the only factor inducing evolution. Therefore, only the intercept of the FP evolves with redshift, while the scatter and slopes remain constant. In this model, for any given redshift, velocity dispersion, effective radius ( $z^i, \sigma^i, r_e^i$ ), and observational errors of an individual galaxy, we can calculate the probability density of the colours, magnitude, and intercept of the FP (defined in Equation 12). By taking into account the selection effects with a MonteCarlo routine (a large number of points are generated and only the ones satisfying the selection criteria are kept) we obtain the probability density  $p^i(\tau | \mathbf{f}^i g)$  of observing  $\mathbf{f}^i$  given  $z_f$ . Since the galaxies are independent samplings of the statistical ensemble we obtain:

$$p(\mathbf{f}^i g | z_f) = p^i(\tau | \mathbf{f}^i g): \quad (32)$$

As in Equation 28, the probability density of  $z_f$  given the set of observations can be computed by assuming an a priori probability density  $p(z_f)$  from the Bayes theorem:

$$p(z_f | \mathbf{f}^i g) = \frac{p(\mathbf{f}^i g | z_f) p(z_f)}{\int p(\mathbf{f}^i g | z_f) p(z_f) dz_f}; \quad (33)$$

In the following, we will assume a constant a priori probability between two values of  $z$ :

$$p(z_f) = p_1 H(z_f - z_m) H(z_M - z_f): \quad (34)$$

A very natural choice is one with  $z_m$  very close to the highest  $z^i$  of the sample and a high value of  $z_M$ , in order to include the interval where  $p^i(\tau | \mathbf{f}^i g)$  is non-zero. We use  $z_m = 0.5$  and  $z_M = 4.0$  for the cosmology and  $z_m = 0.5$  and  $z_M = 10.5$  for the classical cosmology.

The a posteriori probability densities are shown in Figures 15 and 16. The probability density peaks at  $z = 1.2$  (8.9 Gyr look-back time) and it extends to  $z = 0.8$  (7 Gyr) and  $z = 1.8$  (11 Gyr) in the cosmology. In the classical cosmology the probability is much flatter and it extends from  $z = 1.5$  (10 Gyr) to the upper limit of the sampled interval (the age of the Universe in this cosmology is 13.1 Gyr). The distributions are computed for a variety of realizations of the model, with different metallicities, IMFs, stellar atmospheres, showing that the result is robust and does not depend on the details of the model.

In order to check the dependence of the results on the a priori probability density we consider the following approach. An alternative and equivalently straightforward a priori probability is the one obtained by considering the look-back time of formation ( $t_f$ ) as the parameter of the model, instead of the redshift of formation ( $z_f$ ) used in Equation 33:

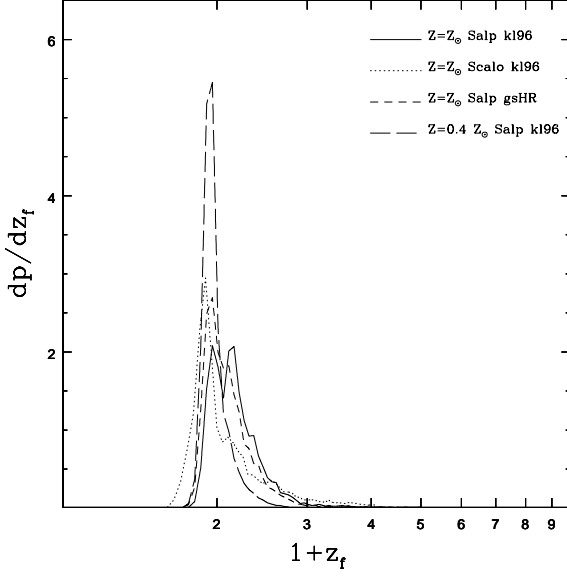


Figure 15. Single-burst stellar population models, I. The probability density of the redshift of formation ( $z_f$ ) of the stellar populations of field early-type galaxies, given the present set of observations, is shown for various realizations of the models. BC 96 spectral synthesis models are used with Salpeter or Scalo IMF, solar or 0.4 solar metallicity, stellar atmospheres from k196 or from gsHR (see Bruzual & Charlot 1996 for details). Independently of the model, the probability density turns out to peak at  $z_f \approx 1$ . The cosmology is assumed. Details of the method are given in Section 6.2.

$$p(t_f | g) = \frac{p(f | g | t_f) p(t_f)}{p(f | g | t_f) p(t_f) dt_f}; \quad (35)$$

Similarly to the case with  $z_f$ , we assume a prior uniform within the interval defined by the look-back time of the most distant galaxy in our sample and the age of the Universe. The posterior  $p(t_f | g)$  can be transformed into the posterior in  $z_f$  in the usual way:

$$p^0(z_f | g) = p(t_f(z_f) | g) \frac{dt_f}{dz_f}; \quad (36)$$

where

$$\frac{dt_f}{dz_f} = \frac{1}{H_0 (1+z_f)^2 \left( \frac{1}{(1+z_f)^3} + \frac{R}{(1+z_f)^2} \right)}; \quad (37)$$

with

$$R = 1 - \Omega_m : \quad (38)$$

Since  $p(f | g | t_f) = p(f | g | z_f)$ , from Equations 33, 35, and 36 it follows that:

$$p^0(z_f | g) / p(z_f | g) = \frac{dt_f}{dz_f}; \quad (39)$$

i.e. the probability density obtained by assuming a prior uniform in  $t_f$  is proportional to the one obtained by assuming a prior uniform in  $z_f$  multiplied by the modulus of the derivative of  $t_f$  with respect to  $z_f$  (the constants are set by requiring that the probability density integrated over  $z_f$  be equal to 1).

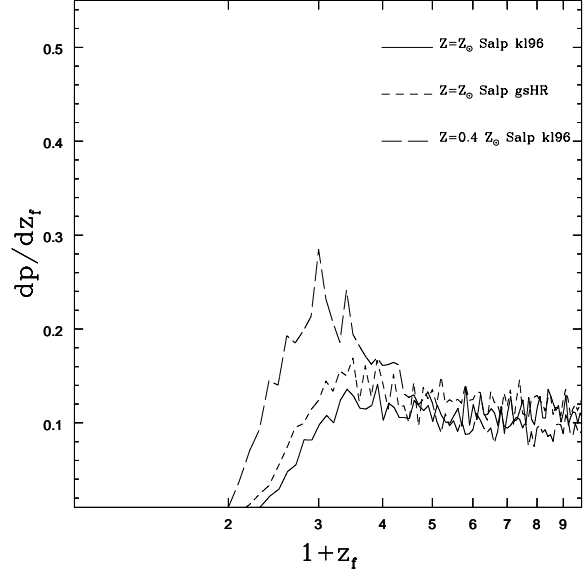


Figure 16. Single-burst stellar population models, II. As in Figure 15, for the classical cosmology.

The resulting a posteriori probability densities are plotted in Figures 17 and 18, respectively for the  $\Lambda$  and the classical cosmology. It is noticed that the a posteriori probability density changes negligibly in the cosmology, while in the classical cosmology the probability density peaks at smaller  $z_f$  and declines at high  $z_f$ . However, this does not alter the physical interpretation of the result, since in any case the stellar populations turn out to be formed long ago ( $> 10$  Gyr). Since the effects of changing the a priori probability density do not alter the physical interpretation of the results, in the following we will present only the results obtained by assuming a prior uniform in  $z_f$ , recalling that the results obtained by assuming a prior uniform in  $t_f$  can be obtained with Equation 39.

### 6.2.3 Secondary bursts of star formation

The single-burst stellar population model is useful as a benchmark to quantify and compare different results. However, it is clearly a simplified picture of the star formation history of early-type galaxies. A small amount ( $< 10$  per cent) of the total mass of moderately young stars (1 Gyr or so) can significantly alter the integrated colours and mass-to-light ratio of an old stellar population for a few Gyr. In this scenario, after a few Gyr, the integrated colours and mass-to-light ratio become totally indistinguishable from the ones of an old single-burst stellar population (see also Jimenez et al. 1999).

A wealth of observations suggest that minor episodes of star formation can occur from intermediate redshifts to the present (e.g. Schade et al. 1999; Trager et al. 2000a; Bernardi et al. 1998). Therefore, it is worth investigating this possibility for our sample of field early-type galaxies. The task can be accomplished by modifying the model described above to allow for a secondary burst of star formation occurred at  $z_{f2} < z_{f1}$ , being  $z_{f1}$  associated with the epoch of the first burst. In this case Equation 33 is changed to

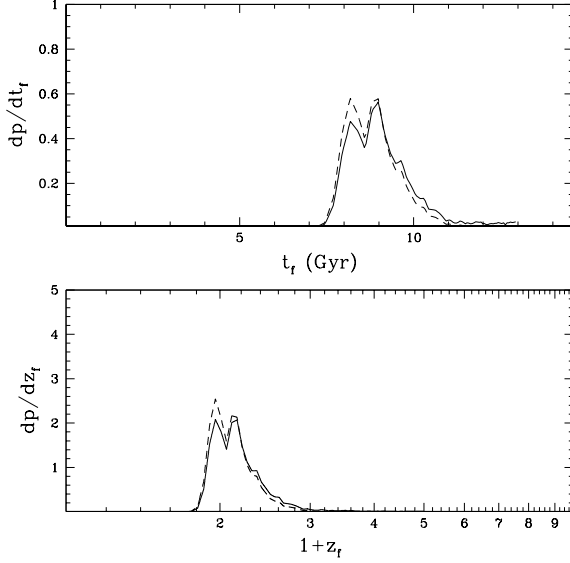


Figure 17. Single-burst stellar population models, III. Effects of the a priori probability density. The a posteriori probability density of the look-back time of formation ( $t_f$ ) and of the redshift of formation ( $z_f$ ) are plotted respectively in the upper and lower panel (cosmology). Dashed lines correspond to a prior uniform in  $t_f$ , solid lines to a prior uniform in  $z_f$ . BC96 spectral synthesis models are used with Salpeter IMF, solar metallicity, and K196 stellar atmospheres. The effects of changing the a priori probability are negligible. A discussion of the a priori probability density is given in Section 6.2.

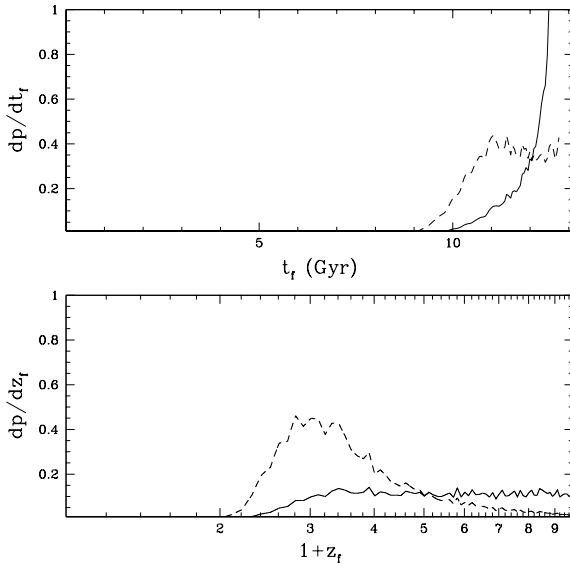


Figure 18. Single-burst stellar population models, IV. As in Figure 17, for the classical cosmology (see Section 6.2).

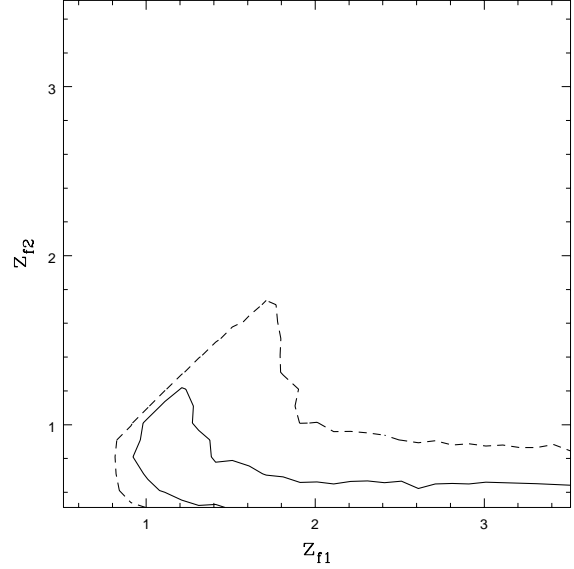


Figure 19. Model with two populations of stars. The older component is formed at  $z_{f1}$ , the younger, with a tenth of the mass, is formed at  $z_{f2}$ . Contour levels of the a posteriori probability are shown as solid (68 per cent) and dashed (95 per cent) lines. The cosmology is assumed. BC96 models with solar metallicity, Salpeter IMF and K196 atmospheres are used.

$$p(z_{f1}; z_{f2} | f^i, g) = \frac{p(f^i | g, z_{f1}; z_{f2}) p(z_{f1}; z_{f2})}{\int p(f^i | g, z_{f1}; z_{f2}) p(z_{f1}; z_{f2}) dz_{f1} dz_{f2}} \quad (40)$$

The a priori probability is assumed to be constant within a test interval

$$p(z_{f1}; z_{f2}) / \int p(z_{f1}; z_{f2}) dz_{f1} dz_{f2} = H(z_{f1} - z_m) H(z_m - z_{f1}) / \int H(z_{f1} - z_m) H(z_m - z_{f1}) dz_{f1} dz_{f2} \quad (41)$$

similarly to the one-dimensional case. The contour levels of the probability density corresponding to 68 per cent and 95 per cent probability are shown in Figure 19 for the cosmology and a mass ratio of the two populations of 10 (the older being 10 times the mass of the younger). Not surprisingly, it is sufficient to have a small mass of stars formed at  $z < 0.6 - 0.8$  to make it possible for the rest of the stellar mass to be formed at the very beginning of the Universe ( $z_{f1} \approx 3 - 4$ , i.e. 12–13 Gyr ago).

It is important to check that such scenario is also consistent with the small scatter of the FP observed at low and intermediate redshift. Since a number of physical phenomena contributes to the scatter of the FP, the scatter due to differences in ages must be smaller than the observed one. In order to simulate this effect we have considered a very simple model, where the bulk of the stellar population is formed at  $z = z_0$  and a secondary burst (of a tenth of the mass) occurs at a later time, with uniform probability between  $z = z_{s1}$  and  $z = z_{s2}$ . The observed trend in  $\sigma$  vs.  $z$  is reproduced without any particular fine-tuning of the parameters ( $z_0 \approx 2 - 3$ ,  $z_{s1} \approx 0.6$ ,  $z_{s2} \approx 0.8$ , for example, work well) and the resulting scatter in  $\sigma$  is very small ( $< 0.01$ ). It is interesting to note that, if we extend to lower redshifts the tail of the secondary burst of star formation, the evolution of  $\sigma$  is not altered significantly, while the scatter induced

by the spread in average age of the stellar populations is comparable to the observed one ( $< 0.08$ ).

### 6.3 Constraining the cosmological parameters

The Bayesian-MonteCarlo approach can be extended also to constrain the cosmological parameters. To this aim, it is sufficient to modify Equation 33 into

$$p(z_f; \mathbf{f}^i | g) = \frac{\int p(\mathbf{f}^i | g, z_f; \mathbf{d}) p(z_f; \mathbf{d}) dz_f}{\int p(\mathbf{f}^i | g, z_f; \mathbf{d}) p(z_f; \mathbf{d}) dz_f}; \quad (42)$$

where, for simplicity, only  $\mathbf{d}$  has been introduced, and to assume a discrete a priori probability using the Dirac distribution

$$p(z_f; \mathbf{d}) = p_1 H(z_f - z_{m1}) H(z_{m1} - z_f) + p_2 H(z_f - z_{m2}) H(z_{m2} - z_f) \quad (43)$$

The normalization factors ( $p_1, p_2$ ) are chosen so that the integral of each term over  $z_f$  and  $\mathbf{d}$  equals 1/2. The intervals in  $z_f$  are chosen as in Section 6.2. The probability density  $p(\mathbf{f}^i | g, z_f; \mathbf{d})$ , is related to the probability densities in Equation 33 by

$$p(\mathbf{f}^i | g, z_f; \mathbf{d}) / p_{0.3}(\mathbf{f}^i | g, z_f) = p_{0.3}(\mathbf{f}^i | g, z_f) / p_{0.3}(\mathbf{f}^i | g, z_f) \quad (44)$$

The probabilities obtained for the two cosmologies are compared in Figure 20. The maximum of probability occurs clearly for the cosmology but the area subtended by the classical cosmology is actually larger (0.3 vs 0.7). Hence, at this redshift, given the present uncertainties on the evolution of the stellar populations, the cosmology is the ‘best-guess’ cosmology, but the classical cosmology cannot be ruled out by this method (see the 68 per cent limits marked with thick lines in Figure 20; see also the discussion by Bender et al. 1998 and van Dokkum et al. 1998b).

### 6.4 Systematic errors

The analysis performed above takes the random errors of the measurement into account. However, we still have to estimate the uncertainty related to global systematic errors, such as:

(i) Zero point errors. We estimate the uncertainty in the absolute zero point of filters F606W and F814W to be  $< 0.03$  mag (see the HST Instrument Handbook and references therein for the listing and description of uncertainties)

(ii) Errors in the K-color correction. These errors are  $0.01 - 0.02$  mag (see P II). As a check, we compared the K-color corrections obtained with our method with the ones derived by Kelson et al. (2000a) and van Dokkum et al. (1998b). We found, consistent with the error estimate, differences  $0.01 - 0.02$  mag.

(iii) Uncertainty in the local FP. The slopes and the zero point of the FP of the Coma cluster are known with errors. The uncertainty on  $\alpha$  for our reference samples (Bender 1998, Lucey 1991) is  $0.01$ , including photometric calibration, K-correction, and foreground extinction. We assume the distance to Coma to be  $cz = 7200 \text{ km s}^{-1}$  and we neglect, as discussed in Section 4, differences between the FP

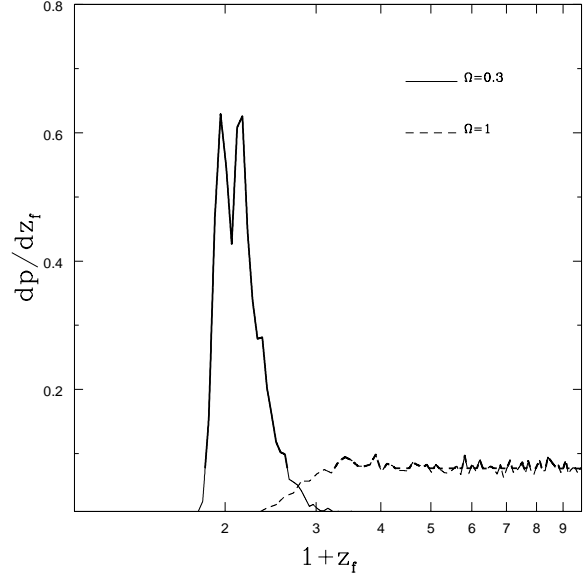


Figure 20. Probability density of the redshift of star-formation given the present set of observations. The a posteriori probability densities for the classical and the cosmology are compared by means of an extension of the Bayesian-MonteCarlo approach (see Section 6.3). The maximum of the probability is for the cosmology. However, the 68 per cent limits (thick lines) include also the classical cosmology.

of Coma and the FP of other clusters or the field. We also neglect possible small differences between the FP in the centre and in the outer parts of Coma (Lucey et al. 1991).

The total systematic error, obtained by adding in quadrature the terms listed above, does not exceed 0.015 in  $\alpha$ . We tested the robustness of our results with respect to this uncertainty by recomputing the probability density for  $\alpha$  after changing the Coma intercept by  $0.015$ . The 68 per cent limits are changed by  $\sim 10$  per cent.

Since the coefficients of the FP and  $SBE-R_E$  relation are measured independently, the very good agreement of the results found in B and V, with the FP and  $SBE-R_E$  relation, is an important check on the accuracy of the photometric calibration and the determination of the local relations.

In principle, it is possible to take into account systematic errors in the Bayesian-MonteCarlo approach. In fact, it is sufficient to treat the photometric zero point, the K-color corrections, and the intercept of the local FP as additional parameters of the model and then integrate over the values of the parameters, as in the following example. Let us denote the set of additional parameters related to the systematic errors as  $\mathbf{f}^i | g$ , and let us assume that their probability distribution are independent  $p(\mathbf{f}^i | g) = \prod_i p(\mathbf{f}^i)$ . Thus, Equation 28 becomes:

$$p(\mathbf{f}^i | g) = \frac{\int \prod_i p(\mathbf{f}^i | g, \mathbf{f}^i | g) p(\mathbf{d}) \prod_i p(\mathbf{f}^i) d\mathbf{f}^i}{\int \prod_i p(\mathbf{f}^i | g, \mathbf{f}^i | g) p(\mathbf{d}) \prod_i p(\mathbf{f}^i) d\mathbf{f}^i}; \quad (45)$$

However, the computational cost of implementing this procedure in our Bayesian-Monte Carlo code<sup>Y</sup> is not justified in our opinion, given the limited knowledge of the systematics, and the other sources of uncertainties that enter the interpretation of the results (see also the next subsection).

### 6.5 Morphological evolution bias

The morphological selection criterion can introduce a bias in our results (the morphological evolution bias described in Section 2.2). For example, one may think (Franx & van Dokkum 1996) that early-type galaxies become morphologically recognizable only after their stellar populations reach a minimum age ( $A_0$ ). In this case, the evolution of the morphologically selected sample would be biased towards an older average age of the stellar population (simply because objects younger than  $A_0$  are discarded).

A simple model where E/S0 form at a random time in a given redshift interval can help quantify the bias. For example, in the Universe, by forming galaxies in the redshift range  $z = 0.5 - 1.5$ , and by considering them as E/S0 only after 3 Gyr, we can reproduce the observed evolution of with constant scatter  $0.06 - 0.07$ .

However, in this scenario no E/S0 would be recognizable at  $z = 1$ , in contrast with the observations (Im et al. 1996; Schade et al. 1999; Treu & Stiavelli 1999). By requiring that at least one third of present-day E/S0 be already assembled and recognizable at  $z = 1$ , we may need a smaller  $A_0$  or an earlier period of formation. Reducing  $A_0$  does not work, since the age component in the scatter of the FP rapidly exceeds the values allowed by the observations. An earlier period of formation is therefore needed. Starting earlier the formation ( $z < 3$  is required) alone does not work either, since the evolution of becomes too slow. In order not to exceed the observed scatter it is necessary to stop forming E/S0 earlier in the Universe. For example, if the formation occurs between  $z = 1$  and  $z = 2$  and  $A_0 = 2$  Gyr, the evolution of is reproduced, the age contribution to the scatter is always smaller than the scatter observed, and 48 per cent of E/S0 are recognizable at  $z = 1$ .

In conclusion, based on the results of the FP alone, we cannot exclude that field E/S0 have been forming until recently ( $z = 0.5$ ) if they become morphologically recognizable only at a moderately old age ( $> 3$  Gyr). In turn, we can exclude this possibility, if we take into account the observational constraint that a significant part of the population of E/S0 is recognizable at  $z = 1$ . With this constraint we are forced to push back the epoch of formation of the stellar populations of field E/S0 to  $z > 1$ .

<sup>Y</sup> In practice the CPU time (a few hours on a Pentium III running at 500 Mhz for the computations shown in Figures 15 to 17) is multiplied by the number of samplings of the distribution of the parameters related to systematic errors. Even by taking only ten samplings per systematic parameter ( $Y^i$ ), the CPU time increases 1000 times.

Table 2. Compilation of sources for FP parameters of galaxies in clusters at intermediate redshift. For each cluster we list the redshift, the rest frame band in which photometry is given, the number of objects per cluster, and the reference. Only objects classified as E/S0 have been considered. See Section 7 for discussion.

Cluster	z	band	nobj	ref
CL1358	0.33	V	30	Kelson et al. 2000b
A 370	0.375	B	7	Bender et al. 1998
MS1512	0.375	B	2	Bender et al. 1998
CL0024	0.39	V	7	van Dokkum & Franx 1996
MS2053	0.58	V	5	Kelson et al. 1997
MS1054	0.83	B	6	van Dokkum et al. 1998b

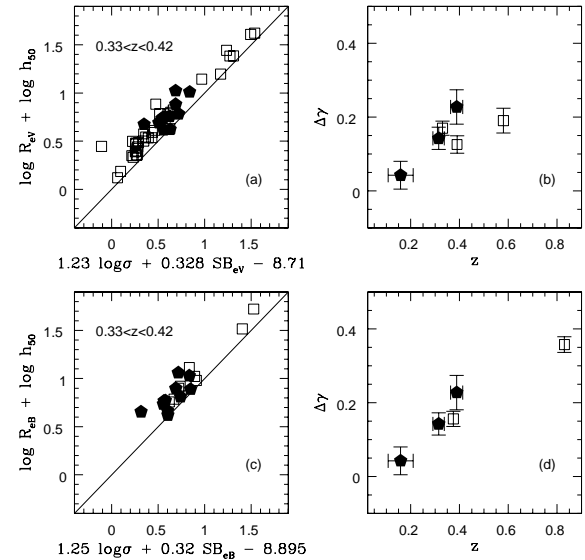


Figure 21. Comparison of field and cluster ellipticals in the FP-space at intermediate redshift. Filled pentagons are field data points from this paper, open squares are cluster data taken from the literature (see Table 2). In panels (a) and (c) the position in the FP-space of galaxies at similar redshift is shown. In panels (b) and (d) the offset of the intercept with respect to Coma is plotted as a function of redshift. The cosmology is assumed. The comparison yields very similar results in the classical cosmology (see Treu 2001).

## 7 COMPARISON BETWEEN FIELD AND CLUSTER RESULTS

In this section we compare the intermediate redshift field FP to a compilation of cluster data taken from the literature (see Table 2).

In Figure 21 we plot the cluster and the field FP data points in the cosmology (the results of the comparison are very similar for the "classical" cosmology and are not shown here, see Treu 2001). In panels (a) and (c) the cluster and field data points at  $0.33 < z < 0.42$ , respectively in the V and B band, are plotted in the FP-space. Panels (b) and (d) illustrate the offset of the intercept with respect to Coma as a function of redshift. The same slopes and have been used for consistency, thus eliminating this source of systematic error in the relative comparison. The data at similar



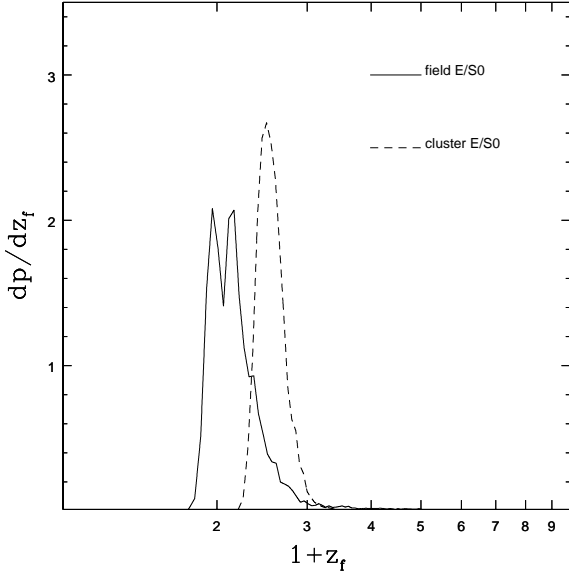


Figure 22. Comparison of the redshift of formation probability density obtained for field (solid line) and cluster E/S0 (dashed line). The cluster data in the B band have been considered (see Table 2). BC96 models with Salpeter IMF, solar metallicity, and  $k196$  atmospheres have been used. The cosmology is assumed.

redshift ( $z \approx 0.3$ – $0.4$ ) provide the following results. The clusters points at  $z = 0.375$  and  $z = 0.39$  (panels b and d) are marginally (1–2 standard deviations) below the field data points, while the point at  $z = 0.33$  is well consistent with the field data points. By applying the Bayesian-Monte Carlo code to recover the a posteriori probability density for the cluster data points, we confirm that: the stellar populations of the galaxies in the two clusters at  $z = 0.375$  and  $z = 0.39$  are marginally older than the ones in the field. On the other hand, the probability distribution obtained for the galaxies in the cluster at  $z = 0.33$  is indistinguishable from the one obtained in the field. We conclude that, given the differences in the selection process (see below), and the size of observational errors, no difference is detected between cluster and field galaxies.

The cluster data points at higher redshift ( $z = 0.58$ – $0.83$ ) show consistently a smaller offset from the local relation than the one that would be extrapolated from the field points. For example, if we apply our Bayesian-Monte Carlo approach to the data in B band out to  $z = 0.83$ , we obtain an older average age for the cluster stellar populations (see Figure 22). A larger sample of field data, extended to higher redshift, is needed in order to perform a more stringent comparison. To this aim, we are currently collecting spectra for 25 galaxies in the redshift range  $z = 0.4$ – $0.7$  using FORS2 on the Very Large Telescope (VLT). We expect that the observational errors on  $\log R_{\text{ev}}$  will be comparable with the ones obtained for the present study. Thus, we will be sensitive to possible differences of 10 per cent between the offset of the intercept for field and cluster E/S0.

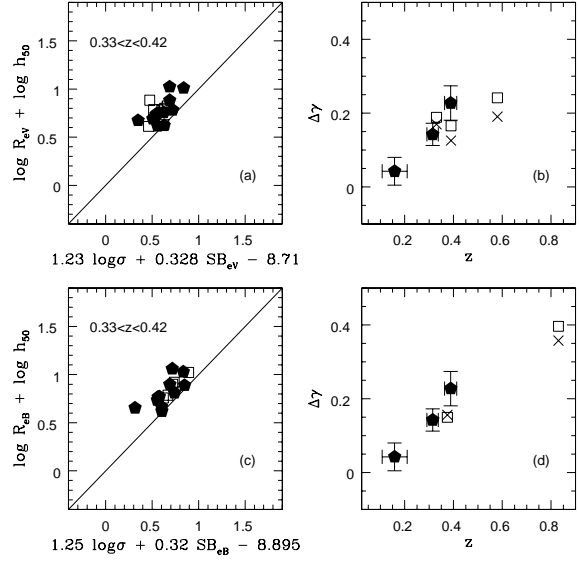


Figure 23. As in Figure 21. Only cluster galaxies in the same ranges of  $\log R_{\text{ev}}$  and  $R_{\text{e}}$  as those of the field sample have been used (open squares). The results found with the complete cluster sample are plotted as crosses for reference.

### 7.1 Sample selection effects

The galaxies in the cluster sample span wider ranges in  $\log R_{\text{ev}}$  and  $R_{\text{e}}$  than those of our sample of galaxies. This effect is related to the lower limit in velocity dispersion measurable by our instrumental setup (see P II) and by the absence of giant objects such as brightest cluster galaxies in our sample. Note that we were not biased against very large (and hence bright) objects. We simply did not find any of them. This selection effect could bias the results if, for example, larger galaxies were older than smaller ones.

The size of this bias can be estimated by comparing the field data to a subsample of cluster E/S0 with  $\log R_{\text{ev}}$  and  $R_{\text{e}}$  within the limits of our sample. This subsample shows a marginally larger offset from the local relation than the complete sample (see Figure 23). However, this result should be taken with great care, since the samples we are considering are very small and the change in the intercepts can be simply due to noise. Larger samples with well controlled selection effects are needed to address the issue whether the evolution of the stellar populations depend on effective mass, possibly with the help of a measurement of a change in the slopes of the FP with redshift.

In addition, the possible bias induced by the cluster population evolution (see Section 2) has to be considered. Phenomena such as the Butcher-Oemler effect (Butcher & Oemler 1984), the evolution of the morphology-density relation (Dressler et al. 1997), or the larger scatter of the colour-magnitude relation of lenticular galaxies, noticed by van Dokkum et al. (1998a) in the outer parts of a cluster at  $z = 0.33$ , seem to suggest that the galaxy population of clusters evolves. Therefore, it is difficult to extend the information gathered by studying the FP in the core of clusters at high redshift to the whole population of present-day clusters. In particular, if galaxies are accreted from the field into

the cluster, the cluster population at intermediate redshift is not the progenitor of the present-day cluster population. Studies with a large field of view, encompassing the entire range of densities from the core of rich clusters to the sparse random fields, are needed before we can clarify how cluster populations evolve and how the environment affects galaxy evolution.

## 8 CONCLUSIONS

In this paper we have studied the Fundamental Plane and the  $SB_e-R_e$  relation for a sample of field early-type galaxies at intermediate redshift. In particular, we have used the FP and  $SB_e-R_e$  as diagnostics of the stellar populations. The main results are:

(i) Evolution of the FP. The FP of field early-type galaxies exists and is tight out to  $z \approx 0.4$ . The scatter is consistent with being unchanged out to  $z \approx 0.4$ . The intercept is offset with respect to that of Coma, in the sense that at a given effective radius and velocity dispersion galaxies are brighter at  $z \approx 0.4$  than in the local Universe. The ranges of  $\sigma$ ,  $SB_e$ , and  $re$  covered by our sample are not sufficient to measure the slopes of the FP at intermediate redshift accurately. Similar results are obtained by studying the  $SB_e-R_e$  relation out to  $z \approx 0.5$ .

(ii) Single-burst stellar populations. In a single-burst scenario, the observed properties of this sample of galaxies are consistent with those of a single-burst stellar population formed at  $z \approx 0.8-1.6$  (cosmology) or at  $z > 2$  (classical cosmology). These redshifts of formation correspond to a present age of 7–11 Gyr or 10–13 Gyr, respectively, in the two cosmologies.

(iii) Multiple-burst stellar populations. If a small fraction of the stellar mass is formed in a secondary burst at a later time, the primary burst may have occurred at high  $z$  even in the cosmology. For example, the data are consistent with the scenario where the primary burst occurred at  $z > 3$  and a secondary burst, with a tenth of stellar mass, occurred at  $z \approx 0.6-0.8$ .

(iv) Field vs. Cluster. No significant difference is found between the Fundamental Plane of field E/S0 at intermediate redshift and that of cluster E/S0 at similar redshift taken from the literature. The ages of the stellar populations of field early-type galaxies inferred from the single-burst model are marginally smaller than the ages derived for samples of cluster early-type galaxies extended to higher redshift. Unfortunately, various selection processes, the small samples available, and the different ranges in global properties spanned by the field and cluster samples do not allow us to draw firm conclusions. Larger sets of data at higher redshift, as the one we are currently collecting with the VLT, are needed to investigate possible differences with higher sensitivity. A larger set of data, sampling a larger range of effective masses and a variety of environments from rich clusters to the field, is also needed to address the issue of the cluster population evolution bias and the possible dependence of the evolution on effective mass.

## 9 ACKNOWLEDGMENTS

This work is based on observations collected at the European Southern Observatory (La Silla) under programmes 62.O-0592, 63.O-0468, and 64.O-0281 and with the NASA/ESA Hubble Space Telescope, obtained at the Space Telescope Science Institute, which is operated by a Association of Universities for Research in Astronomy, Inc. (AURA), under NASA contract NAS5-26555. Tommaso Treu was financially supported by the Space Telescope Science Institute Director Discretionary Research Fund grant 82228, and by the Italian Ministero dell'Università e della Ricerca Scientifica e Tecnologica. Giovanni Punzi is thanked for useful discussions on Bayesian Statistics.

## REFERENCES

- Abraham R. G., Ellis R. S., Fabian A. C., Tanvir N. R., Glazebrook K., 1999, *MNRAS*, 303, 641
- Barger A. J., Cowie L. L., Trentham N., Fulton E., Hu E. M., Songaila A., Hall D., 1999, *AJ*, 117, 102
- Bayes Rev. T., 1763, *Phil. Trans. Roy. Soc.*, 53, 370
- Bender R., Burstein D., Faber S. M., 1992, *ApJ*, 399, 462
- Bender R., Ziegler B., Bruzual G., 1996, *ApJ*, 463, L51
- Bender R., Saglia R. P., Ziegler B., Belloni P., Greggio L., Hopp U., Bruzual G., 1998, *ApJ*, 493, 529
- Bender R., Burstein D., Faber S. M., 1993, *ApJ*, 411, 153
- Benítez N., Broadhurst T., Bouwens R., Silk J., Rosati P., 1999, *ApJ*, 515, L65
- Berger J. O., 1999, Institute of Statistics and Decision Sciences Discussion Paper 99-30, Duke University
- Bernardi M., Renzini A., da Costa L. N., Wegner G., Alonso M. V., Pellegrini P. S., Rite C., Wilmer C. N. A., 1998, *ApJ*, 508, L43
- Binggeli B., Sandage A., Tarenghi M., 1984, *AJ*, 89, 64
- Bower R. G., Lucey J. R., Ellis R. S., 1992, *MNRAS*, 254, 601
- Brimicombe J., Ellis R. S., 2000, *ApJ*, 536, L77
- Brown T., Bowers C. W., Kimbers R. A., Ferguson H. C., 2000, *ApJ*, 529, L89
- Bruzual A. G., Charlot S., 1993, *ApJ*, 405, 538
- Butcher H., Oemler A., 1984, *ApJ*, 285, 426
- Capaccioli M., Caon N., D'Onofrio M., 1992, *MNRAS*, 259, 323
- Chiba M., Yoshi Y., 1999, *ApJ*, 510, 42
- Ciotti L., Lanzoni B., Renzini A., 1996, *MNRAS*, 282, 1
- Daddi E., Cimatti A., Pozzetti L., Hoekstra H., Rottgering H. J. A., Renzini A., Zamorani G., Mannucci F., 2000, *A&A*, 361, 535
- Djorgovski S., Davis M., 1987, *ApJ*, 313, 59
- Dressler A., Lynden-Bell D., Burstein D., Davies R. L., Faber S. M., Terlevich R. J., Wegner G., 1987, *ApJ*, 313, 42
- Dressler A. et al., 1997, *ApJ*, 490, 577
- Ellis R. S., Smail I., Dressler A., Couch W. J., Oemler A., Butcher H., Sharples R. M., 1997, *ApJ*, 483, 582
- Faber S. M., Jackson R. E., 1976, *ApJ*, 204, 668
- Faber S. M., Dressler A., Davies R. L., Burstein D., Lynden-Bell D., 1987, in Faber S. M., ed., *Nearly Normal Galaxies*. Springer, New York, p. 175
- Fish R. A., 1964, *ApJ*, 139, 284
- Franceschini A., Silva L., Fasano G., Granato L., Bressan A., Aumouts S., Danese L., 1998, *ApJ*, 506, 600
- Franx M., van Dokkum P. G., 1996, in Bender R., Davies R. L., eds., *Proc. IAU Symp. 171, New Light on Galaxy Evolution*. Kluwer, Dordrecht, p. 233
- Graham A., Colless M., 1997, *MNRAS*, 287, 221
- Gri ths E. et al. 1994, *ApJ*, 435, L19
- Groth E. J., Juskiewicz R., Ostriker J. P., 1989, *ApJ*, 346, 558

- Im M., Gri ths R. E., Ratnatunga K. U., Sara jedini V. L., 1996, *ApJ*, 461, L79
- Je reys H., 1961, *Theory of Probability*, Oxford University Press
- Jimenez R., Friaca A. C. S., Dunlop J. S., Terlevich R. J., Peacock J. A., Nolan L. A., 1999, *MNRAS*, 305, L16
- J rgensen I., Franx M., Kj rgaard P., 1996, *MNRAS*, 280, 167
- J rgensen I., Franx M., Hj rth J., van Dokkum P. G., 1999, *MNRAS*, 308, 833
- Kau mann G., 1996, *MNRAS*, 281, 487
- Kau mann G., White S. D. M., Guiderdoni B., 1993, *MNRAS*, 264, 201
- Kelson D. D., van Dokkum P. G., Franx M., Illingworth G. D., Fabricant D., 1997, *ApJ*, 478, L13
- Kelson D. D., Illingworth G. D., van Dokkum P. G., Franx M., 2000a, *ApJ*, 531, 137
- Kelson D. D., Illingworth G. D., van Dokkum P. G., Franx M., 2000b, *ApJ*, 531, 184
- Kodama T., Bower R. G., Bell E. F., 1999, *MNRAS*, 305, 561
- Kormendy J., 1977, *ApJ*, 218, 333
- Larson R. B., 1975, *MNRAS*, 173, 671
- Lucrey J. R., Guzman R., Carter D., Terlevich R. J., 1991, *MNRAS*, 253, 584
- Menanteau F., Ellis R. S., Abraham R. G., Barger A. J., Cowie L. L., 1999, *MNRAS*, 309, 208
- Pahre M. A., 1998, PhD Thesis, California Institute of Technology
- Pahre M. A., De Carvalho R. R., Djorgovski S. G., 1998a, *AJ*, 116, 1606
- Pahre M. A., Djorgovski S. G., De Carvalho R. R., 1998b, *AJ*, 116, 1591
- Perlmutter S. et al., 1999, *ApJ*, 517, 565
- Postman M., Lubin L. M., Gunn J. E., Oke J. B., Hoessel J. G., Schneider D. P., Christensen J. A., 1996, *AJ*, 111, 615
- Renzini A., Ciotti L., 1993, *ApJ*, 416, L49
- Salpeter E., 1955, *ApJ*, 121, 161
- Scalo J., 1986, *Fund Cosmic Phys.*, 11, 1
- Schade D., Barrientos L. F., Lopez-Cruz O., 1997, *ApJ*, 477, L17
- Schade D. et al., 1999, *ApJ*, 525, 31
- Scodeggio M., Gavazzi G., Belsole E., Pierini D., Boselli A., 1998, *MNRAS*, 301, 1001
- Stanford S. A., Eisenhardt P. R., Dickinson M. E., 1998, *ApJ*, 492, 461
- Toomre A., 1977, in Tinsley B. T., Larson R. B., eds., *The Evolution of Galaxies and Stellar populations*. Yale University Press, New Haven, p.401
- Trager S. C., Worthey G., Faber S. M., Burstein D., Gonzalez J. J., 1998, *ApJS*, 116, 1
- Trager S. C., Faber S. M., Worthey G., Gonzalez J. J., 2000a, *AJ*, 119, 1645
- Trager S. C., Faber S. M., Worthey G., Gonzalez J. J., 2000b, *AJ*, 120, 165
- Treu T., 2001, Ph.D Thesis, Scuola Normale Superiore.
- Treu T., Stiavelli M., 1999, *ApJ*, 524, L27
- Treu T., Stiavelli M., Casertano S., Miller P., Bertin G., 1999, *MNRAS*, 308, 1037 (T99)
- Treu T., Stiavelli M., Miller P., Casertano S., Bertin G., 2001, *MNRAS*, in press (P II), astro-ph/0104177
- van Albada T. S., 1982, *MNRAS*, 201, 939
- van Albada T. S., Bertin G., Stiavelli M., 1995, *MNRAS*, 276, 1255
- van Dokkum P., Franx M., 1996, *MNRAS*, 281, 985
- van Dokkum P., Franx M., Kelson D. D., Illingworth G. D., Fisher D., Fabricant D., 1998a, *ApJ*, 500, 714
- van Dokkum P., Franx M., Kelson D. D., Illingworth G. D., 1998b, *ApJL*, 504, L17
- van Dokkum P., Franx M., Fabricant D., Illingworth G. D., Kelson D. D., 2000, *ApJ*, 541, 95
- White S. D. M., Rees M. J., 1978, *MNRAS*, 183, 341